An Improved method to generate secondary nanoplastics and oligomers: Application in ecotoxicology

Silvia Gómez-Kong, Miguel Tamayo-Belda, Gerardo Pulido-Reyes, Carlos Edo, Irene Verdú, Francisco Leganés, Roberto Rosal, Miguel González-Pleiter, Francisca Fernández-Piñas. Environmental Science Nano 12, 1150-1165, 2025.

https://doi.org/10.1039/D4EN00866A

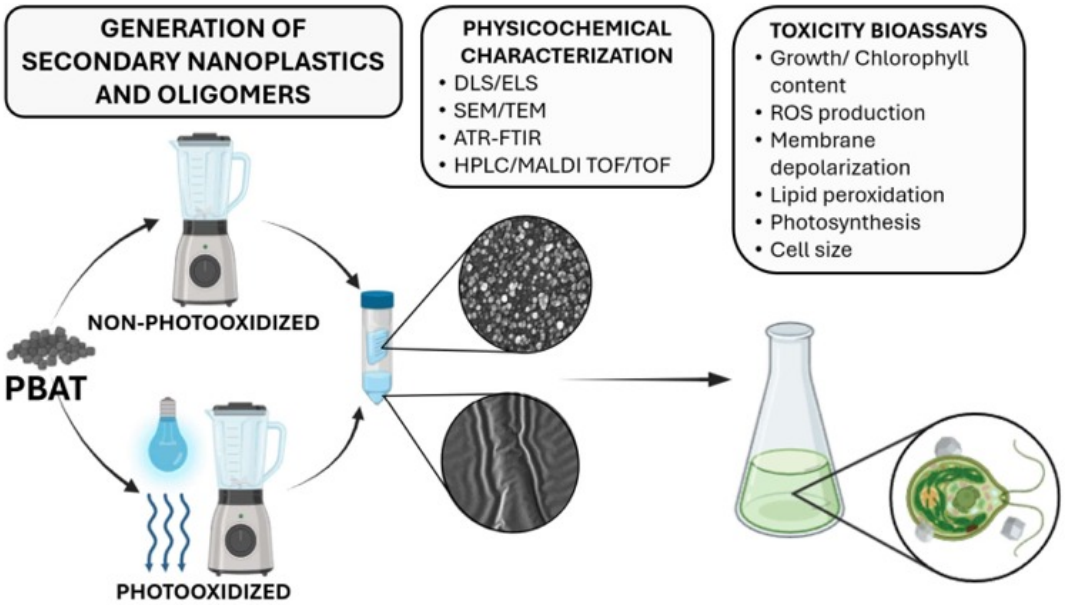

An Improved method to generate secondary nanoplastics and oligomers: Application in ecotoxicology

Silvia Gómez-Kong[1], Miguel Tamayo-Belda[1], Gerardo Pulido-Reyes[1], Carlos Edo[2], Irene Verdú[1], Francisco Leganés[1,3], Roberto Rosal[2], Miguel González-Pleiter[1,3], Francisca Fernández-Piñas[1,3,*]

[1]Department of Biology, Faculty of Science, Universidad Autónoma de Madrid, E-28049, Madrid, Spain
[2]Department of Chemical Engineering, Universidad de Alcalá, E-28871 Alcalá de Henares, Madrid, Spain
[5]Centro de Investigación en Biodiversidad y Cambio Global (CIBC-UAM), Universidad Autónoma de Madrid. Darwin 2, 28049 Madrid, Spain

Abstract

Recent studies have highlighted the ecotoxicological effects of conventional primary nanoplastics (NPLs), however, the impacts of secondary NPLs and oligomers (Olig), especially those derived from biodegradable plastics, formed through fragmentation and natural degradation processes (e.g., photooxidation) remain underexplored. This gap is partly due to challenges in producing sufficient quantities for toxicity testing. An improved method to generate non-photooxidized (NP) and photooxidized (P) secondary NPLs and Olig from polybutylene adipate co-terephthalate (PBAT), a biodegradable plastic commonly used in agriculture mulching, that involves the mechanical breakdown of PBAT-microbeads with or without prior photooxidation is presented. PBAT was irradiated at ∼9.34 kW m^{-2} (approximately 120 times the solar irradiance) during 96 h, irradiation that corresponds to ∼16 months of average sunlight in the Iberian Peninsula (7.7 kWh m^{-2} day^{-1}). The toxicological effects on *Chlamydomonas reinhardtii*, a model green microalga of primary producers in freshwater ecosystems was also assessed. The protocol yielded 0.199 mg of secondary NP-PBAT-NPLs and 10.275 mg of NP-PBAT-Olig per gram of PBAT-microbeads. PBAT-NPLs presented irregular spherical morphologies and hydrodynamic sizes ranging from 56.71 to 69.86 nm. HPLC and MALDI-TOF analysis identified linear and cyclic Olig, ranging from dimers to 19 repeated-units Olig. PBAT-NPLs and PBAT-Olig exhibited negative surface charges, suggesting colloidal stability in water. While PBAT-NPLs and PBAT-Olig did not inhibit algal growth in the short-term, they induced reactive oxygen species overproduction at the environmentally relevant concentrations of 0.01 mg/L, and caused membrane depolarization, impaired photosynthesis and lipid peroxidation at 10 mg/L. Non-photooxidized PBAT-NPLs exhibited the highest toxicity, followed by photooxidized PBAT-NPLs and both non-photooxidized and photooxidized PBAT-Olig. This study provides an efficient method for producing reference secondary NPLs and Olig and underscores the potential risks of PBAT towards primary producers in freshwater ecosystems.

1 Introduction

In total, 1925 million tons of plastics were produced worldwide between 2018 and 2022, excluding quantities used for adhesives, sealants, coatings, paints, varnishes, textiles, waterproofing, or those for the production of cosmetics and medicines[1]. Notably, approximately 90 % of these plastics derived from fossil fuels, while less than 9 % originated from the recycling processes. During this same period, the production of bio-based plastic doubled, reaching 2.3 million tons in 2022. The majority of plastics are utilized in packaging, which typically results in a short product lifespan. Once discarded, plastic waste can follow several pathways: recycling (only for some types and a limited number of times), landfill disposal, energy recovery or released into the environment Upon entering either directly or after undergoing one or more of these processes. Recente estimations suggest that between 0.8 to 2.7 Mt enter the ocean each year and 80 % of them are transported by rivers threatening freshwater ecosystems[2].

Freshwater ecosystems serve as key pathways for the transport of plastic waste into the environment[3]. Upon entering the ecosystems, they undergo fragmentation and natural degradation processes due to factor such as light (producing photooxidation), temperature (producing thermal oxidation), water (producing hydrolysis) or mechanical forces, with the latter generally considered the most efficient abi-

* Corresponding author: francisca.pina@uam.es
Available online: December 23, 2024

otic degradation procedure[4]. Exposure to visible and ultraviolet radiation increases the plastic reactivity by promoting electron excitation, which accelerates oxidation, cleavage, and chain scission, leading to the formation of smaller particles in the nanometer range[5]. These particles, known as nanoplastics (NPLs) are plastic particles < 1000 nm in one dimension[6]. NPLs frequently appear together with oligomers (Olig: short polymeric chains) that are released during the same degradation process and may be isolated by ultrafiltration through 50 kDa MWCO (molecular weight cut-off)[7,8]. On the one hand, particles smaller than 1000 nm tend to remain as stable colloidal systems unless the particles exhibit neutral surface charge. Absolute ζ-potential values of 20-30 mV or higher are generally accepted to maintain colloidal stability[9]. On the other hand, the behaviour of molecules is influenced by several factors, mainly their interaction with the surrounding solvent that may promote their solubility or more frequently, in aqueous media, their hydrophobic-driven self-aggregation[10]. Furthermore, NPLs and Olig can be categorized by origin into primary which are intentionally manufactured, such as those found in personal care products, and secondary resulting from fragmentation and degradation of macro and microplastics into nanosized particles[11].

Research on the presence of NPLs in the environment remains limited due to the technical challenges associated with their identification and quantification in complex matrices[12,13]. To date, the presence of NPLs in the environment has been analyzed using different techniques such as adapted thermal desorption proton transfer reaction mass spectrometry (TD-PTR-MS)[14−19] and pyrolysis gas chromatography mass spectrometry (Py-GC/MS)[20−22]. The concentration of NPLs in different water bodies ranges from 0.1 μg/ L in river waters, groundwater and WWTP water effluents in China to an extreme value of 1,588 μg/L in a Swedish lake[17,20−22]. Despite these findings and the potential higher degradation rates of biodegradable NPLs, there is currently no evidence of biodegradable NPLs or oligomers in the environment[23].

Due to these barriers for NPLs identification and aiming at evaluating the physicochemical behavior and biological toxicity of NPLs in complex matrixes, some studies have focused on generating different type of NPLs to tackle these handicaps. Most of them have applied a variety of bottom-up method to obtain NPLs for different applications: testing different materials such as PMMA (poly(methyl methacrylate) or PHB (polyhydroxybutyrate)[24,25]; making the NPLs trackable [26,27] and with more realistic irregular shapes[28,29]. There exist alternatives for top-down methods producing more realistic NPLs by mechanical fragmentation of larger plastics in different liquid media as well as through laser ablation[30−33]. These alternatives have allowed the use of different materials in the NPLs toxicology but also bring to light the lack of standardized methodologies to produce high quantities of realistic NPLs of reference that behave in a similar way that those naturally occurring in the environment as a consequence of the degradation processes of larger plastics[4].

Once NPLs reach the environment, they can exert negative effects on organisms. To the best of our knowledge, so far there have not been described effects of secondary NPLs, at environmentally relevant concentrations, on the viability of organisms but they have been described for more sensitive endpoints such as specific metabolic alterations and behavioral changes[32−34]. In this regard, environmental risk could be underestimated. In general, toxicological studies about NPLs have predominantly focused on evaluating a few types of primary NPLs such as PS (polystyrene), PE (polyethylene) and PMMA[35−41]. In comparison, conventional polymers and biopolymers appear to exert similar toxicity[42]. However, the faster degradation of the biopolymers, with the greater release of additives, and their effects on the biota and their balance may jeopardize to a greater extent the stability of the ecosystems[43,44]. Only a limited number of scientific articles have examined the impact of secondary NPLs or/and biodegradable plastics like PCL (polycaprolactone)[8], PHB[7,25] and PLA (polylactic acid)[32]. The uncontrolled release of plastic oligomers has been considerably studied as non-intentionally added substances in food contact materials[45], but their impact on the environment is an issue that has yet to be addressed.

Taken together, while there is a rapidly growing body of evidence on the presence of NPLs in the environment and the negative effects of primary NPLs, the standard method to detect NPLs in complex matrices are still under development and the studies assessing the effects of secondary NPLs and Olig (especially those derived from biodegradable plastics) formed through fragmentation and natural degradation processes (e.g., photooxidation) remain scarce. These knowledge gaps are partly due to the challenges of producing sufficient quantities for toxicity and analytical testing. Here, we have developed a highly efficient method to generate both non-photooxidized and photooxidized secondary NPLs and Olig from polybutylene adipate co-terephthalate (PBAT), a biodegradable plastic commonly used in agriculture mulching, that can be adapted to other polymers. Our novel method involves the mechanical breakdown of pristine PBAT-microbeads, with

or without prior photooxidation. The toxicological effects on *Chlamydomonas reinhardtii* (*C. reinhardtii*), a model green microalga of primary producers in freshwater ecosystems was also assessed.

2 Materials and methods

2.1 Nanoplastics and oligomers production

Secondary non-photooxidized (NP-) PBAT nanoplastics (PBAT-NPLs) and PBAT oligomers (PBAT-Olig) have been produced by mechanical breakdown of commercial PBAT microbeads purchased from Ecoflex with an average molecular number of 50 kDa[46]. 300 g of commercial microbeads were frozen by liquid nitrogen at -140 °C, triturated in a modified stainless-steel blender Thermomix TM31 (Vonwerk, Germany) equipped with four stainless-steel blades and load capacity of 1.3 L (Supplementary Text S1, Fig. 1). The trituration was carried out for 1 minute at a speed of 10,000 rpm and passed through a 1 mm sieve, to isolate the smaller fractions. 10 trituration cycles were done only in the plastic fraction > 1 mm. At the end of the trituration procedure, approximately 70 % of the plastic was smaller than 1 mm. 15 g of the pulverized plastic < 1 mm were collected, resuspended in 20 mL of absolute ethanol and 60 mL of ultra-pure water and then ultrasonicated on a Branson Ultrasonics Sonifier S-450A (Branson Ultrasonics Co., Brookfield, CT, USA) for 2 min at 60 % duty cycle and 260 W. Then the resuspended fraction was filtered using a 1 µm pore nylon filter. Fractions below 1 micron were concentrated, and the oligomeric fraction was separated by centrifuge ultrafiltration using a 50 kDa MWC membrane. Both, fraction between 5-1000 nm and fraction < 5 nm (50 kDa MWCO), hereinafter NP-PBAT-NPLs and NP-PBAT-Olig respectively were dried in a previously cleaned oven used only for this purpose at 60 ºC for 48 hours, and then, and then weighted, using a balance (accuracy ± 0.01 mg), and stored in 4 mL glass flasks for later use.

Secondary photooxidized (P-) PBAT nanoplastics (PBAT-NPLs) and PBAT oligomers (PBAT-Olig) were produces as follows: 100 g of commercial PBAT microbeads were place into a glass bottle filled with 800 ml of absolute ethanol and then radiated with a 150 W medium-pressure mercury lamp (Novalight TQ150) emitting in the 297–579 nm 172 range during 96 h (Text S1 Fig. 2), irradiation that corresponds to 16 months of average sunlight in the Iberian Peninsula (7.7 kWh m^{-2} day^{-12})[47]. After radiation, microbeads were filtered, dried and the same protocol for the production of NP-PBAT-NPLs and NP-PBAT-Olig was conducted. Detailed information about the protocols described above is available in the Supplementary Material (Text S1).

2.2 Physicochemical characterization

2.2.1 Dynamic lightscattering (DLS) and electrophoretic light scattering (ELS)

The hydrodynamic size and surface charge (inferred using the ζ-potential) of the colloidal suspension of NP- and P-PBAT-NPLs and NP- and P-PBAT-Olig was determined by DLS and ELS using a Zetasizer Nano ZS (Malvern Instruments, Malvern, UK). Measurements were performed at 25 °C in ultra-pure water and in the corresponding culture medium used for the biological study. A working suspension of 1000 mg/L of each material were used. Additionally, to investigate the influence of the culture medium in the NPLs dispersion, the same concentrations were prepared in the appropriate culture medium. DLS measurements were replicated five times with eleven runs per replicate, while ELS measurements were replicated five times with thirty runs per replicate

2.2.2 Transmission and scanning electron microscopy (TEM/SEM)

For transmission electron micrographs, 10 µL of 1000 mg/L PBAT-NPLs suspension were placed on a carbon film coated, 400 Mesh, nickel grid support and dehydrated at room temperature to fix the material on the grid. Post-fixation was performed in osmium tetroxide in phosphate buffer for 2 h at 4 °C. Samples were stained with 2 % uranyl acetate. PBAT-NPLs were visualized on a JEOL (JEM 1010) electron microscope (80-120 kV). For scanning electron images (SEM), working suspensions of 100 mg/L of NP- and P-PBAT- NPLs or PBAT-Olig were prepared from which 10 µL were placed on an aluminum holder, dehydrated at room temperature and coated with 5 nm of chromium. Samples were studied using an Electron Beam Lithography eLINE-Plus equipment (Raith, Germany).

2.2.3 Fourier transform infrared spectroscopy (FTIR)

The identification of the chemical structure of PBAT-NPLs and PBAT-Olig obtained at different stages of the production process were performed by Attenuated Total Reflectance Fourier Transform Infrared (ATR-FTIR) spectroscopy. Commercial PBAT microbeads, fragmented material below 1 mm obtained after mechanical breakdown, nanoparticle samples and oligomer samples were analysed and compared. PBAT-NPLs and PBAT-Olig samples were dried at 60 °C and placed over ATR-crystal. For the microbeads, a slice was cut and placed over ATR-crystal. Spectra were taken in the 4000-500 cm^{-1} range. The analysis was conducted on a Perkin-Elmer Spotlight 200 Spec-

trum Two apparatus equipped with an MCT detector (PerkinElmer, USA). The IR spectra were analysed using Origin software (OriginLab Corporation, USA).

2.2.4 High-performance liquid chromatography (HPLC) and matrix-assisted laser desorption/ionization (MALDI) time-of-flight/time-of-flight (TOF/TOF) mass spectrometry

Considering the wide variety of oligomers that may potentially appear in the NP- and P-PBAT-Olig samples, the characterization of this fraction was conducted in two steps: separation by polarity of the different oligomeric compounds present in the raw NP- and P-PBAT-Olig material generated (which mainly depends on the hydrocarbon chain length and monomer composition) followed by individual MALDI-TOF/TOF analysis of each peak obtained in the first step. Chromatographic separation of the raw NP- and P-PBAT-Olig material was conducted using an HPLC 1200 Series Agilent apparatus (Agilent Technologies, Germany) equipped with an autosampler and ultraviolet diode array detector. The raw material was separated on an Ace Excel 5 CN-ES, (250 x 4.6 mm, 5 µm) column with 100 % methanol as mobile phase at a flow rate of 1 mL/min by a 0-20 min gradient. The material was injected at 20 mg/mL and analysed at 254 nm. Oligomeric chains length and structure were assessed by mass spectrometry with MALDI-TOF/TOF configuration and NdYAG laser (355 nm) ULTRAFLEX III (Brunker Daltoniks GmbH, Bremen, Germany). MALDI TOF/TOF analyses were performed essentially as described by Tamayo-Belda et al.[7]. Each chromatography peak corresponding to PBAT-Olig was dissolved in methanol from which 5 µL of each of the solutions were mixed with 20 µL of trans-2-[3-(4-tert-butylphenyl)-2-methyl-2-propenylidene] malononitrile (DCTB) matrix solution (8 mg/mL in dichloromethane) and 0.5 µL of sodium iodide (2 mg/mL in acetone). Before analysis, 0.5 µL of this mixture was placed on the MALDI sample plate to dry at room temperature. Recordings were conducted in positive ion detection mode in the range of 50 to 5000 Da for the most polar peaks and 600 to 5000 Da for the less polar peaks to gain sensitivity. Analyses were performed using FlexAnalysis software (Bruker) complemented with the optimization tool Excel Solver (Microsoft).

2.3 Toxicity assays

The unicellular green microalga *C. reinhardtii* was obtained from the Culture Collection of Algae and Protozoa of Dunstaffnage Marine Laboratory (Scotland, UK) and routinely cultured in in six-fold diluted TAP culture medium adjusted at pH 7 and buffered with 3.3 mM Tris(hydroxymethyl)aminomethane (TRIS) and 45 mM phosphate buffer (TAP/6), which has been used as appropriate culture medium for growing *C. reinhardtii* in a rotary shaker, at 135 rpm and 28 °C under continuous light of 40 µmol photons m^{-2} s^{-1} as described elsewhere[48]. The initial OD_{750nm} for the exposure experiment was 0.15. Microalgae were exposed for 72 h to (1) NP- and P-PBAT-NPLs and (2) NP- and P-PBAT-Olig at different nominal concentrations, hereinafter, concentrations (0.01; 0.1; 1; 10; and 50 mg/L). Microalgae exposed to the same concentrations of pure ethanol used to resuspend both NPLs and Olig were used as controls (0.01 % v/v). Five replicates of controls and three replicates of each treatment were carried out. After 72 h of exposure, cellular growth, and total content of chlorophyll (Chl *a* + Chl *b*) were measured. For cellular growth, absorbance at 750 nm was measured. For chlorophyll contents, the photosynthetic pigments were extracted in acetone (90 %) at 4 °C for 24 h in darkness, and the absorbance at 664 and 647 nm for Chl *a* and Chl *b*, respectively was measured. The concentration of chlorophylls was determined according to Jeffrey and Humphrey[49]. pH of the culture medium with and NP- and P-PBAT-Olig was measured after 96 h to ensure no toxic effects were observed due to the medium acidification (Table S1).

2.3.1 Flow cytometry assays

The mechanisms of action of NP- and P-PBAT-NPLs and NP- and P-PBAT-Olig on the alga were measured in *C. reinhardtii* cultures, exposed for 72 h at the concentrations of 0.01; 0.1; 1; 10; and 50 mg/L of each fraction, in triplicate using flow cytometry (FCM) in a CytoFLEX S Flow Cytometer (Beckman Coulter) fitted with violet (405 nm), blue (488 nm), yellow-green (561 nm), and red (638 nm) lasers. Size was detected with forward scatter (FSC), and blue laser with three detectors with different wavelength intervals were used: a 488/8 nm detector of side scatter (SSC), 525/40 nm (FITC), and 690/50 nm (PerCP). Besides size (FSC), complexity (SSC) and chlorophyll autofluorescence (PerCP), two fluorescent probes (FITC) were used to evaluate two physiological parameters (incubation times and concentrations were adapted from Tamayo-Belda et al.[50]: dihydrorhodamine 123 (DHR 123) for the measurement of intracellular reactive oxygen species (ROS), and bis-(1,3-dibutylbarbituric acid) trimethine oxonol, $DiBAC_4(3)$ for the detection of changes in cytoplasmic membrane potential. Specific nformation on concentration, incubation times and channels are described in Table S2. All fluorochrome stock solutions were prepared in dimethyl sulfoxide and stored at -20 °C. Fluorescence was analysed in logarithmic mode and at least 20,000 gated cells with similar sizes and complexities were evaluated. Three independent ex-

periments with six controls and three samples by treatment were carried out for each parameter. Data acquisition and processing were performed using CytExpert software (Beckman).

2.3.2 Lipid peroxidation

Lipid peroxidation was determined by quantifying thiobarbituric acid reactive substances (TBARS) as described elsewhere with minor modifications[51]. *C. reinhardtii* cells were centrifugated (10000 rpm) and resuspended in 1 mL of 0.5 % thiobarbituric acid (TBA) in 20 % trichloroacetic acid (TCA). The mixture was heated at 90 °C in a hot block for 30 min. Next, samples were centrifuged at 12000 rpm for 10 min. The absorbance of the supernatant was measured at 532 nm. The value for nonspecific absorbance at 600 nm was subtracted. The amount of TBARS was calculated using the extinction coefficient of 155 mM^{-1} cm^{-1}. Five replicates of controls and three replicates of each treatment were carried out. Results were expressed as the percentage of malondialdehyde (MDA) content with respect to the control.

2.3.3 Photosynthesis

The measurement of the photosynthetic oxygen evolution was performed at 28 °C exposing the cells to saturating actin light (300 µmol photons m^{-2} s^{-1}) in a Clark-type oxygen electrode (Hansatech) according to Leganés et al.[52]. Five replicates of controls and three replicates of each treatment were carried out. Photosynthetic rates were relativized to total chlorophyll content and represented as percentage with respect to the control.

2.4 Data analysis

For the biological assays, means and standard errors were calculated from three independent replicate experiments. All values were corrected for control values to minimise the effects of external factors. To determine significant differences among test treatments, data were statistically analysed by conducting an overall one-way analysis of variance (ANOVA) using SigmaPlot v11.0 software (Systat Software Inc., USA). $p < 0.05$ was considered statistically significant. When significant differences were observed, Dunnet's multiple comparation post-hoc test were run for comparing treatments and controls.

3 Results

3.1 PBAT-NPLs and PBAT-Olig characterization

The physicochemical characterization of PBAT-NPLs in terms of size, morphology, surface charge, chemical nature and mass was performed by dynamic light scattering (DLS), scanning electron microscope (SEM-EDX), electrophoretic light scattering (ELS), Fourier transform infrared spectroscopy (FTIR) and dry weight analysis.

Hydrodynamic size and ζ-potential measurements were carried out in ultra-pure water and culture medium in absence of cells (Table 1). The concentration used for measurements was 100 mg/L for all different treatments. DLS measurements in ultrapure water of both NP- and P-PBAT-NPLs hydrodynamic size, transformed in number distribution, have mean sizes of 64 ± 5 nm. In the case of NP-PBAT-Olig particles, mean sizes where 94 ± 7 nm and 170 ± 8 nm for P-PBAT-Olig, indicating the aggregation of NP- and P-PBAT-Olig in a micellar way due to the high hydrophobicity of the material. Regarding ELS measurements, ζ-potential of NP- and P-PBAT-NPLs were -34 mV and -35 mV respectively in ultra-pure water at pH 7, indicating a stable colloidal suspension; and -21 mV and -26 mV for NP- and P-PBAT-Olig respectively, indicating the stability of the micellar aggregates of PBAT-Olig.

The NP-PBAT-NPLs sizes found by DLS in ultrapure water (Table 1; Fig. S1) were also observed by TEM (Fig. 1A; Fig. 1B) while in P-PBAT-NPLs some particles seem to be larger probably due to their aggregation during the sample preparation process. Both NP- and P-PBAT-NPLs SEM images revealed irregular sphere morphologies, while NP- and P-PBAT-Olig SEM images showed a layer of an oily phase without any visible particle.

The comparative infrared spectra of PBAT microbeads, NP- and P-PBAT-NPLs and NP- and P-PBAT-Olig (Fig. 2) showed characteristics peaks of PBAT. The peaks at 2960 and 2873 cm^{-1} are due to asymmetric and symmetric stretching vibrations for CH_2 groups, respectively. Main shoulder of carbonyl region (1720 cm^{-1}) is due to strongly C=O stretch, meanwhile 1732 cm^{-1} peak corresponds to C=O stretch in carbonyl groups in amorphous region of the polymer; the latter is absent in NP- and P-PBAT-Olig. Peak at 1455 cm^{-1} is characteristic from C-C stretch in phenylene group. Peaks at 1410 and 1390 cm^{-1} are due to trans –CH_2– plane bending vibrations and strong peaks at 1268 cm^{-1} correspond to C-O asymmetric stretch. Finally, peaks at 870 and 730 cm^{-1} are due to the out of the plane phenyl ring bending[53].

The formulas, structure and lengths of the polymeric series found by MALDI-TOF/TOF in the NP- and P-PBAT-Olig samples are compiled in the Table 2. The polymeric series composition varies depending on the structure (linear or cyclic); on the number of butylene-terephthalate units inserted into

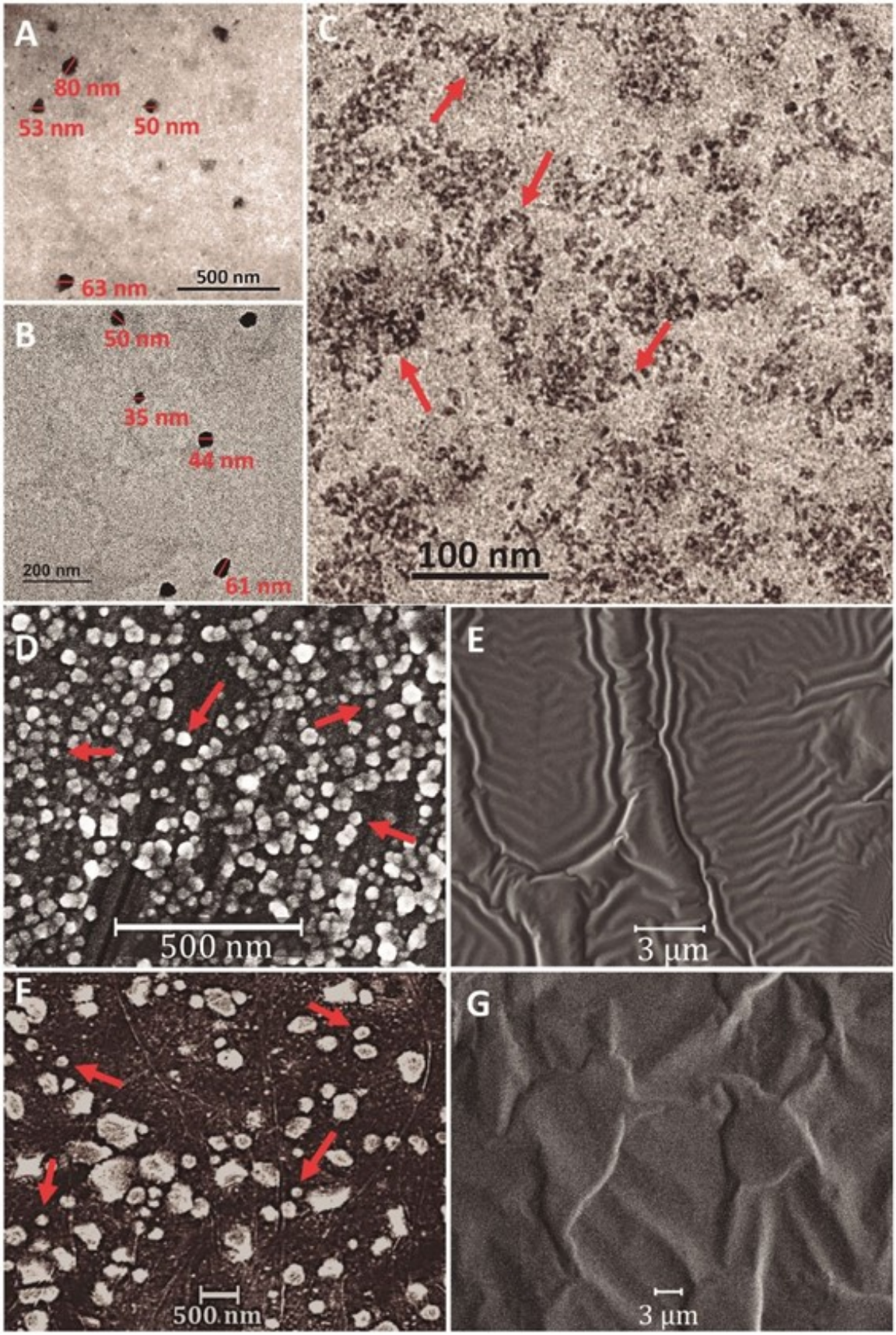

Figure 1: *Transmission electron microscopy (TEM) image of NP-PBAT-NPLs (A). TEM 366 image of P-PBAT-NPLs (B). TEM image of NP-PBAT-Olig (C). Scanning electron microscopy (SEM) image of NP-PBAT-NPLs (D). SEM image of NP-PBAT-Oligomers (D). SEM image of P-PBAT-NPLs (F). SEM image of P-PBAT-Oligomers (G). Red arrows indicate individual particles.*

Table 1. *Hydrodynamic size ($Size_H$), polydispersity index (PdI) and ζ-potential of NP and P-PBAT-NPLs and NP- and P-PBAT-Olig both in ultrapure water and algal culture medium (TAP/6). Data obtained from 3 independent replicates ± standard deviation. Size distribution curves are available in the Supplementary Material (Fig. S1).*

	Ultrapure water			Culture medium		
	$Size_H$ in number (nm)	PDI	ζ-potential (mV)	$Size_H$ in number (nm)	PDI	ζ-potential (mV)
NP-PBAT-NPLs	64 ± 5	0.28	-34 ± 2	94 ± 7	0.33	-41± 3
P-PBAT-NPLs	64 ± 5	0.21	-35 ± 2	60 ± 3	0.21	-36 ± 2
NP-PBAT-Olig	94 ± 7	0.33	-21 ± 3	96 ± 3	0.21	-26 ± 1
P-PBAT-Olig	170 ± 8	0.08	-26.0 ± 0.2	170 ± 7	0.06	-45 ± 1

the oligomers; on the abundance on butylene by-products (butane or butanediol); as well as on the occurrence of additional carbonyl/hydroxyl groups due to oxidation processes. Both types of PBAT-Olig, non-protoxidized and protoxidized, contained oligomeric material below 4000 Da. The mean molecular weight of the NP-PBAT-Olig (1971 ± 116 Da) was significantly higher than that of the P-PBAT-Olig (1635 ± 133 Da) as well as the maximum monomer number observed, which reached 19 units in the non-photooxidized and 15 in the photooxidized one. Based on the MALDI-TOF/TOF intensity output (Fig. S2; Fig. S3), the smallest oligomer observed, the butylene adipate cyclic dimer, was the most abundant in both the first HPLC peak of NP and P-PBAT-Olig and reflects an order of magnitude higher of cyclic dimer abundance after photooxidation. The proportion of carbonyl/hydroxyl groups appearing on the polymeric series increased after photooxidation from 11 % in NP-PBAT-Olig up to 26 % in P-PBAT-Olig. The butylene-terephthalate (BT) was found to be randomly distributed in the polymer. The BT occurrence frequency was approximately 20 % more frequent in the NP-PBAT-Olig with respect to the P-PBAT-Olig one. As shown in Fig. S4, the increase of BT units in the oligomers positively correlated ($R2 \simeq 0.86$) with the time retained in the HPLC, therefore, it is correlated with the hydrophobicity. From the NP-PBAT-Olig, eight consecutive peaks were obtained after 20 min run, while only six from the P-PBAT-Olig after the same time.

3.2 Effects of NP- and P-PBAT-NPLs and NP- and P-PBAT-Olig on physiological endpoints of *C. reinhardtii*

Exposure of *C. reinhardtii* to NP- and P-PBAT-NPLs and NP- and P-PBAT-Olig for 72 h did not significantly alter the growth (Fig. S5) and chlorophyll content (Fig. S6) of the microalga (Dunnet's test, $p < 0.05$); thus, the highest observed-no-effect concentration (HONEC) was 50 mg/L of PBAT-NPLS and PBAT-Olig. Raw data is available in the Supplementary Material (Table S3; Table S4). Although no significant effects were found on growth of the alga when exposed for 72 h to NP- and P-PBAT-NPLs and NP- and P-PBAT-Olig (short-term exposure), sublethal effects could be happening that in the long term may cause damage to the cells; to shed light on that, mechanisms of toxic action were investigated. One of the common responses reported in ecotoxicological studies involving NPLs is the formation of reactive oxygen species (ROS) and oxidative stress. ROS overproduction can lead to an imbalance between intracellular ROS species and the antioxidant mechanisms of the cell. To investigate whether NP- and P-PBAT-NPLs and NP- and P-PBAT-Olig treatments could induce ROS formation and eventually oxidative stress in *C. reinhardtii* cells, flow cytometry (FCM) analyses to assess the formation of H_2O_2 using the fluorescent dye DHR123 was performed. Results showed a significant increase in H_2O_2 intracellular levels (129 %; $p < 0.01$) after 72 h exposure to 0.01 mg/L, the lowest tested concentration, of NP-PBAT-NPLs (Fig. 3A). This response appeared to increase constantly at concentrations ranging from 1 mg/L (122 %; $p < 0.05$), to 10 mg/L (135 %; $p < 0.001$) and 50 mg/L (154 %; $p < 0.001$) (in Fig. 3B, cell subpopulations P1 in green are healthy cells and P2 in blue are cells affected by ROS overproduction). P-PBAT-NPLs caused similar alterations in H2O2 intracellular levels, causing a significant and constant increase at 1 mg/L (119 %; $p < 0.05$), 10 mg/L (127 %; $p < 0.001$), and 50 mg/L (137 %; $p < 0.001$) (Fig. 3A). Nevertheless, ROS formation (hydrogen peroxide) increased to a lesser extent when cells were exposed to NP- and P-PBAT-Olig. The oligomeric fraction only caused a significant ROS overproduction at 10 mg/L (118 %; $p < 0.01$) with further increases at 50 mg/L (129 %; $p < 0.001$) in the case of NP-PBAT-Olig; and at 50 mg/L (128 %; $p < 0.001$) after P-PBAT-Olig exposure (Fig. 3A).

Cytoplasmatic membrane potential has also been analysed by FCM using the fluorochrome $DiBAC_4(3)$

Table 2. *Non-photooxidized NP- and photooxidized P-PBAT-Olig assigned based on MALDI-TOF/TOF spectra. BA:Butylene-Adipate; BT: Butylene-Terephthalate; BH_2: 388 Butanediol; C_4H_{10}: Butane; H_2O: Water or hydroxyl and proton; CO: ketone group (C=O). MALDI-TOF/TOF spectrum of PBAT-Olig chromatography peaks is available in the Supplementary Materia,l Fig. S1 for NP-PBAT-Olig and Fig. S2 for P-PBAT-Olig.*

NP-PBAT-Olig			P-PBAT-Olig		
Formula	Structure	Number of repeating units	Formula	Structure	Number of repeating units
$(BA)_n$	Cyclic	2/1-4	$(BA)_n$	Cyclic	2
$(BA)_n$-(C_4H_{10})	Linear	1-5/2	$(BA)_n$-(C_4H_{10})	Linear	2-4
$(BA)_n$-(BH_2)	Linear	1-8	$(BA)_n$-(BH_2)	Linear	2-9
$(BA)_n$-(BT)-(BH_2)	Linear	1-7/5-12	$(BA)_n$-(H_2O)	Linear 2-8	
$(BA)_n$-(BT)	Cyclic	1-4/2-8	$(BA)_n$-(BH_2)-(CO)	Linear	2-7
$(BA)_n$-$(BT)_2$-(BH_2)	Linear	3-10	$(BA)_n$-(H_2O)-(CO)	Linear	2-6
$(BA)_n$-$(BT)_3$-(BH_2)	Linear	2-9/4-11	$(BA)_n$-(BT)-(BH_2)]	Linear	1-8
$(BA)_n$-(BT)-(C_4H_{10})	Linear	2-6	$(BA)_n$	Cyclic	2-6
$(BA)_n$-$(BT)_2$	Cyclic	0-5/8-10/3-9	$(BA)_n$-(BT)	Cyclic	1-3
$(BA)_n$-$(BT)_4$-(BH_2)	Linear	2-7/7-13/6-12	$(BA)_n$-(C_4H_{10})	Linear	2-9
$(BA)_n$-$(BT)_7$-(BH_2)	Linear	3-8	$(BA)_n$-(BT)-(C_4H_{10})	Linear	2-4
$(BA)_n$-$(BT)_6$-(BH_2)	Linear	5-9	$(BA)_n$-(BT)-(BH_2)	Linear	2-10
$(BA)_n$-$(BT)_2$-(C_4H_{10})	Linear	3-7	$(BA)_n$-$(BT)_2$-(BH_2)	Linear	2-5
$(BA)_n$-$(BT)_3$]	Cyclic	0-8/1-5	$(BA)_n$-(BT)-(H_2O)	Linear	2-7
$(BA)_n$-$(BT)_5$-(BH_2)	Linear	3-9	$(BA)_n$-$(BT)_2$	Cyclic	1-7
$(BA)_n$-$(BT)_4$-(BH_2)	Linear	6-12	$(BA)_n$-(BT)	Cyclic	2-8
$(BA)_n$-$(BT)_3$-(BH_2)	Linear	11-14	$(BA)_n$-$(BT)_4$-(H_2O)	Linear	1-4
$(BA)_n$-$(BT)_9$-(BH_2)	Linear	2-5	$(BA)_n$-(BT)-(C_4H_{10})	Linear	6-11
$(BA)_n$-$(BT)_7$-(BH_2)	Linear	8-11	$(BA)_n$-$(BT)_3$-(BH_2)-(CO)	Linear	8-13
$(BA)_n$-$(BT)_2$-(C4H10)	Linear	6-9	$(BA)_n$-$(BT)_5$-(C4H10)	Linear	2-6
$(BA)_n$-$(BT)_3$-(C4H10)	Linear	4-8	$(BA)_n$-$(BT)_3$-(BH_2)	Linear	4-9
$(BA)_n$-(BT)-(C4H10)	Linear	8-13	$(BA)_n$-$(BT)_4$-(BH_2)	Linear	5-9
$(BA)_n$-$(BT)_5$-(BH_2)	Linear	6-11	$(BA)_n$-$(BT)_2$-(BH_2)	Linear	6-12
$(BA)_n$-$(BT)_6$-(BH_2)]	Linear	4-7	$(BA)_n$-$(BT)_2$-(BH_2)-(CO)	Linear	5-7
$(BA)_n$-$(BT)_5$]	Cyclic	2-5/6-9	$(BA)_n$-$(BT)_6$-(BH_2)	Linear	5-8
$(BA)_n$-(BT)-(H_2O)]	Linear	2-9	$(BA)_n$-$(BT)_2$-(H_2O)	Linear	6-11
$(BA)_n$-$(BT)_2$-(H_2O)	Linear	1-8	$(BA)_n$-$(BT)_3$	Cyclic	1-5
$(BA)_n$-$(BT)_4$	Cyclic	0-9	$(BA)_n$-$(BT)_2$	Cyclic	4-8
BA)$_n$-$(BT)_6$	Cyclic	7-11	$(BA)_n$-$(BT)_4$-(BH_2)	Linear	6-7
$(BA)_n$-$(BT)_7$-(H_2O)	Linear	2-4	$(BA)_n$-$(BT)_5$-(BH_2)	Linear	5
$(BA)_n$-$(BT)_7$	Cyclic	6-9	$(BA)_n$-$(BT)_3$	Cyclic	0-7
$(BA)_n$-$(BT)_8$	Cyclic	5-6	$(BA)_n$-$(BT)_3$-(CH_3OH)	Linear	0-7
$(BA)_n$-$(BT)_4$-(H_2O)	Linear	2-9	$(BA)_n$-$(BT)_2$	Linear	8-10
$(BA)_n$-$(BT)_3$-(H_2O)	Linear	4-10	$(BA)_n$-$(BT)_5$-(BH_2)	Linear	5-8
$(BA)_n$-$(BT)_6$	Cyclic	0-8/6-8	$(BA)_n$-$(BT)_4$-(BH_2)	Linear	8-9

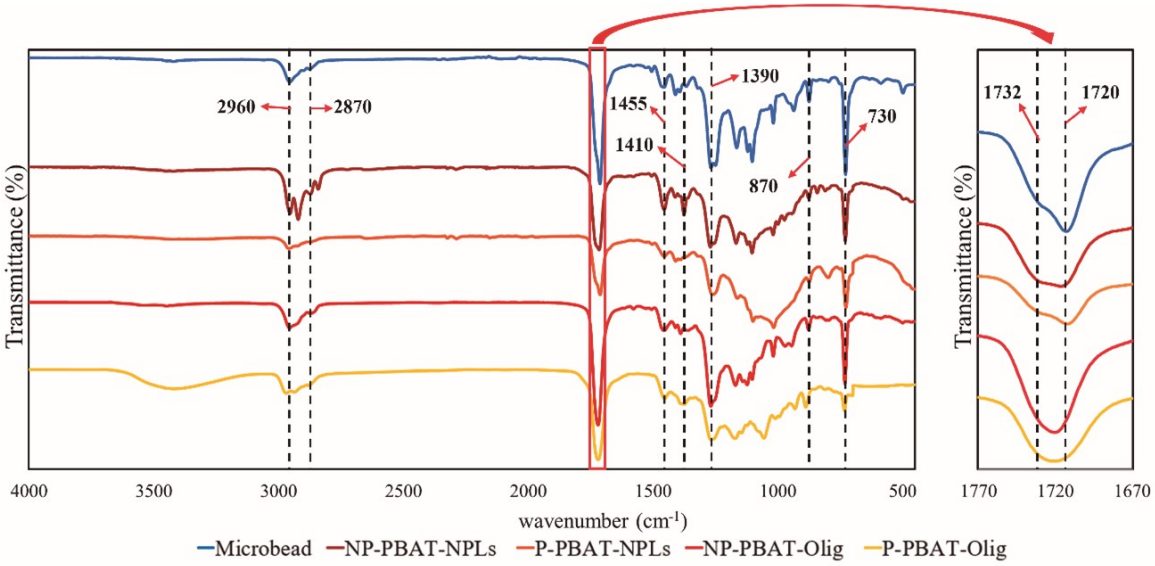

Figure 2: *Infrared spectra of NP- and P-PBAT-NPLs and NP- and P-PBAT-Olig and the initial material (PBAT microbeads).*

(Fig. 4). A significant increase in $DiBAC_4(3)$-stained cells is indicative of a greater fluorochrome influx to the cells; this uptake of $DiBAC_4(3)$ indicates membrane depolarization. Our results showed an increase in membrane depolarization after cell exposure for 72 h in all treatments, being this increase significant at 10 mg/L of NP-PBAT-NPLs (125 %; $p < 0.05$) and at the highest tested concentration, 50 mg/L of NP- (154 %; $p < 0.001$) and P- (131 %; $p < 0.001$) PBAT-NPLs; and NP- (127 %; $p < 0.01$) and P- (122 %; $p < 0.01$) PBAT-Olig respectively (Fig. 4A) (in Fig. 4B, cell subpopulations P1 in green are healthy cells, P2 in orange are cells affected by membrane depolarization and P3 in purple are cells affected by membrane hyperpolarization). No significant decrease in fluorescence was observed, therefore, the exposure did not cause membrane hyperpolarization of the microalga.

ROS overproduction can trigger lipid peroxidation by attacking carbon-carbon double bounds in lipids. Due to their double bounds, polyunsaturated lipids, which are principal components of cell membranes, are prone to oxidant attack, leading to malondialdehyde (MDA) formation as predominant by-product. MDA content can be measured by its reaction with thiobarbituric acid (TBA), which leads to the formation of MDA-TBA2 so called TBARS, a conjugate that absorbs in the visible spectrum at 532 nm and produces a red-pink colour. Thus, an increase in TBARS (expressed here as the percentage of MDA) is associated with membrane lipid peroxidation.

As shown in Fig. 5, a significant increase in MDA levels was caused by the exposure of algal cells to all treatments, with a significant increase at 10 mg/L (141 %; $p < 0.05$) and 50 mg/L (152 %; $p < 0.05$) of NP-PBAT-NPLs and 50 mg/L (145 %; $p < 0.05$) of P-PBAT-NPLs. Regarding exposure of cells to PBAT-Olig, both NP- and P induced a slight but non-significant increase in MDA levels at 50 mg/L exposure (128 % and 127 %; $p < 0.05$ for NP- and P-PBAT-Olig respectively).

The main physiological function of *C. reinhardtii* cells is photosynthesis, therefore, to investigate whether NP- and P-PBAT-NPLs and NP- and P-PBAT-Olig had any effect on this crucial parameter, the photosynthetic activity measured as oxygen evolution in two sublethal intermediate concentrations of NP- and P-PBAT-NPLs and NP- and P-PBAT-Olig was evaluated. The two chosen concentrations were 0.1 mg/L, which already caused significant ROS overproduction but still without effect on membrane potential and lipid peroxidation levels, and 10 mg/L, which caused alterations in these parameters. These concentrations were used to test the effects of 72 h cell exposure to NP- and P-PBAT-NPLs and NP- and P-PBAT-Olig. (Fig. 7). All the treatments caused a decrease ~10 % ($p < 0.05$) in photosynthetic activity at 0.1 mg/L exposure by 72 h and a significant decrease of ~16 % ($p < 0.01$ for NP- and P-PBAT-NPLs; $p < 0.05$ for P-PBAT-Olig) at 10 mg/L. This decrease was not observed after exposure to NP-PBAT-Olig.

Some authors have reported a relationship between pollutants exposure and cell size increase in *C. reinhardtii* cells. We selected the two intermediate concentrations (0.1 and 10 mg/L) to test the effects of 72 h exposure to NP- and P-PBAT-NPLs and NP- and P-PBAT-Olig on *C. reinhardtii* cells. As shown in Fig. 7, *C. reinhardtii* cells treated with 0.1 mg/L of NP- (Fig. S7B) and P- (Fig. S7E) PBAT-NPLs showed no significant differences in cell size, however, there was significant cell size increase after exposure to 10 mg/L NP- (Fig. S6C) and P- (Fig. S6F) PBAT-NPLs

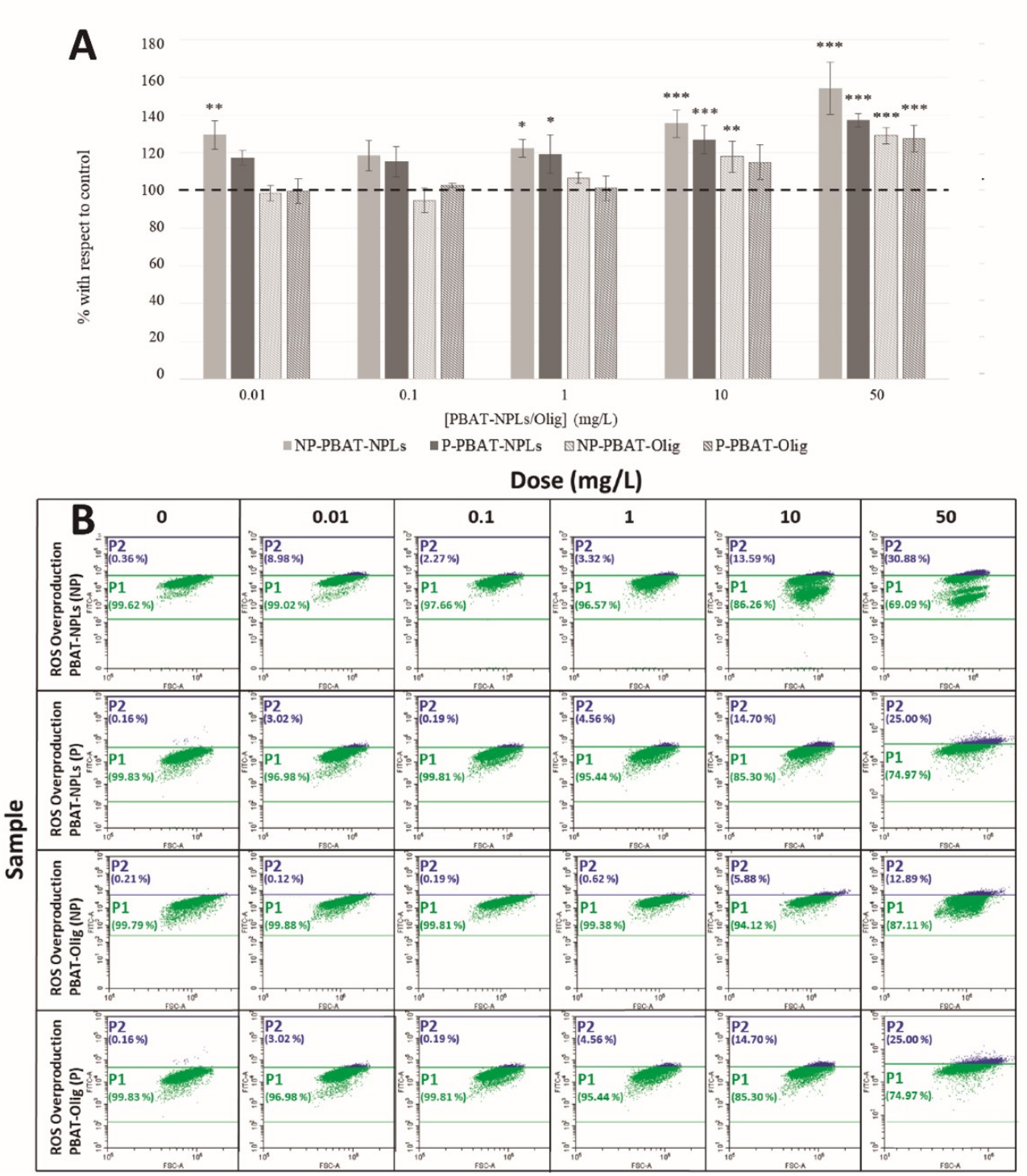

Figure 3: *Percentage of variation with respect to control using the mean of fluorescence intensity for ROS production after exposure to NP- and P-PBAT-NPLs and NP- and P-PBAT-Olig (A). Asterisks indicate treatments that are significantly different (Dunnet's test, *** $p < 0.001$.; ** $p < 0.01$.; * $p < 0.05$) from the control represented as 100 % (dotted line). Representative flow cytometry dot-plots showing ROS overproduction in C. reinhardtii after 72 h exposure to NP- and P-PBAT-NPLs and NP- and P-PBAT-Olig; reactive oxygen species (ROS) was assessed in P1 in green (healthy cells) and P2 in blue (cells affected by ROS overproduction) (B). Raw data is available in the Supplementary 454 Material (Table S5)*

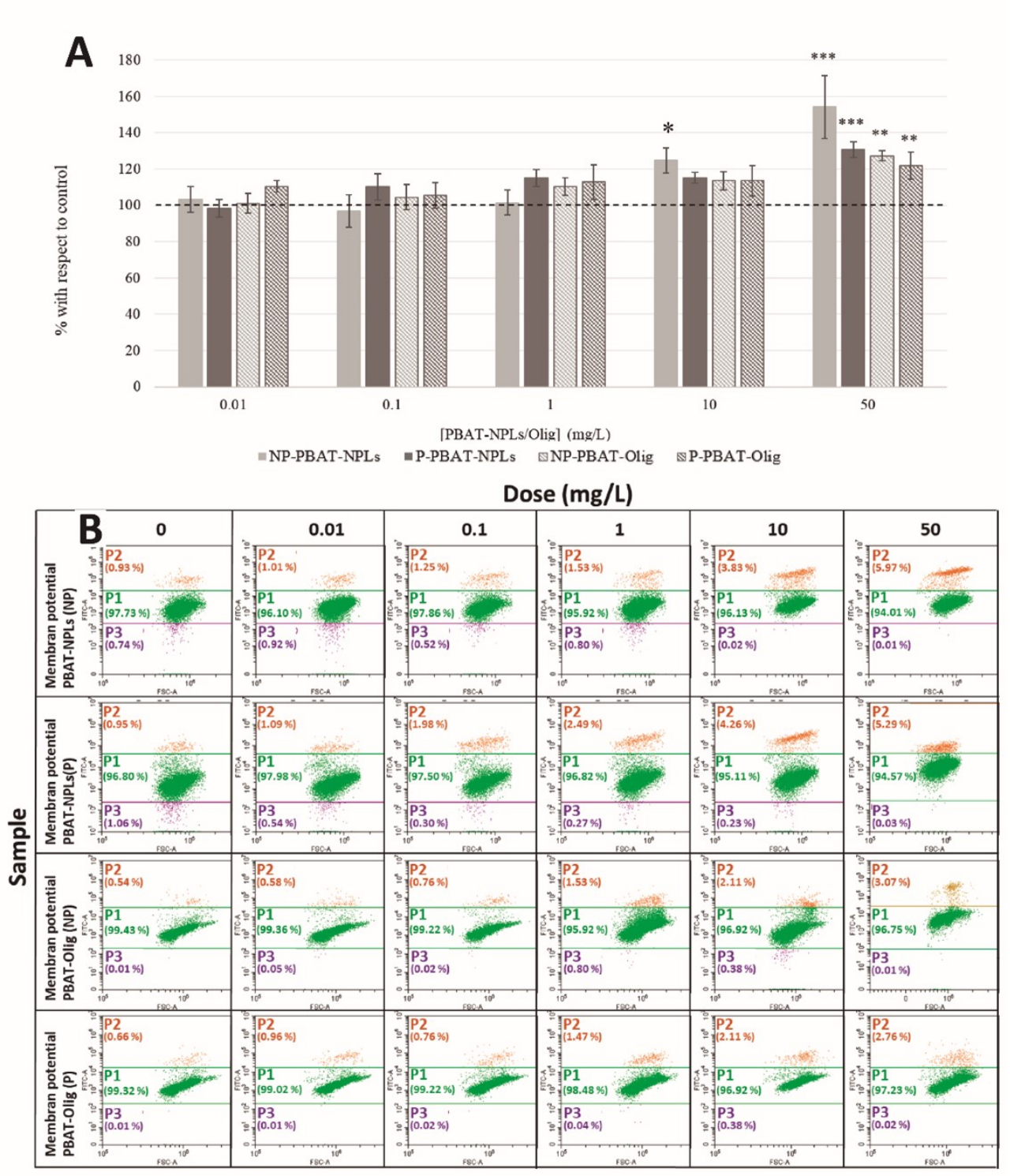

Figure 4: *Percentage of variation with respect to control using the mean of fluorescence intensity for membrane depolarization after exposure to NP- and P-PBAT-NPLs and NP- and P-PBAT-Olig (A). Asterisks indicate treatments that are significantly different (Dunnet's test, *** $p < 0.001$.; ** $p < 0.01$.; * $p < 0.05$) from the control represented as 100 % (dotted line). Representative flow cytometry dot-plots showing alterations of membrane potential in C. reinhardtii after 72 h exposure NP- and P-PBAT-NPLs and NP- and P-PBAT-Olig; cytoplasmatic membrane potential was assessed in three gates: P1 in green (healthy cells), P2 in orange (cells affected by membrane depolarization) and P3 in purple (cells affected by membrane hyperpolarization) (B). Raw data is available in the Supplementary Material (Table S6).*

(106 %; $p < 0.05$). No differences in cell size were observed for exposures to 0.1 and 10 mg/L of NP- and P-PBAT-Olig (Fig. 7).

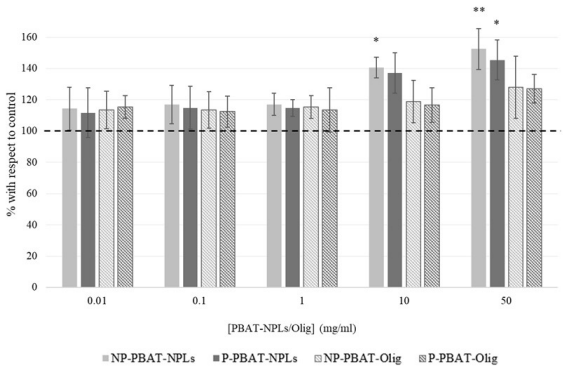

Figure 5: *Lipid peroxidation, measured by thiobarbituric acid reactive substances method (TBARS), on C. reinhardtii after 72 h exposure to NP- and P-PBAT-NPLs and NP- and P-PBAT-Olig. Asterisks indicate treatments that are significantly different (Dunnet's test, *** $p < 0.001$.; ** $p < 0.01$.; * $p < 0.05$) from the control represented as 100 % (dotted line). Raw data is available in the Supplementary Material (Table S7).*

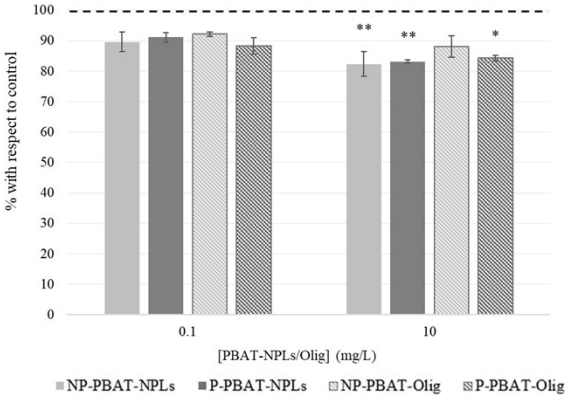

Figure 6: *Oxygen evolution of C. reinhardtii after 72 h exposure to NP- and P-PBAT-NPLs and NP- and P-PBAT-Olig. Asterisks indicate treatments that are significantly different (Dunnet's test, *** $p < 0.001$.; ** $p < 0.01$.; * $p < 0.05$) from the control represented as 100 % (doted line). Raw data is available in the Supplementary Material (Table S8).*

Overall, short term (72 h) exposure of *C. reinhardtii* to NP-PBAT-NPLs induced significant ROS overproduction at the lowest concentration tested of 0.01 mg/L (Fig. 3; Table S5) and NP- and P-PBAT-NPLs caused significant membrane depolarization (Fig. 4; Table S6), lipid peroxidation (Fig. 5; Table S7), impaired photosynthesis (Fig 6; Table S8) and increase of the cell size (Fig. 7: Fig. S7; Table S9) at 10 mg/L. NP- and P-PBAT-Olig showed fewer toxic effects but also triggered significant ROS overproduction (Fig. 3; Table S5), membrane depolarization (Fig. 4; Table S6) at the highest concentrations tested of 50 mg/L and

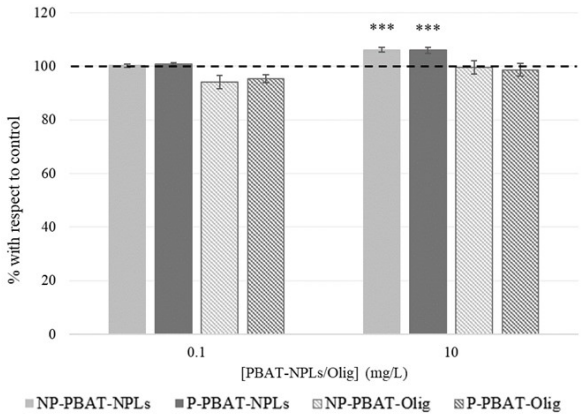

Figure 7: *Cell size based on flow cytometry back scatter of C. reinhardtii after 72 h exposure to NP- and P-PBAT-NPLs and NP- and P-PBAT-Olig. Asterisks indicate treatments that are significantly different (Dunnet's test, *** $p < 0.001$.; ** $p < 0.01$.; * $p < 0.05$) from the control represented as 100 % (dotted line). Raw data of cell size based in flow cytometry is available in the Supplementary Material (Table S9).*

P-PBAT-Olig impaired photosynthesis (Fig. 6; Table S8) at 10 mg/L. All these alterations in the long term may cause significant damages to the algal cells that may compromise their viability eventually causing detrimental effect on the aquatic trophic chain.

4 Discussion

In this work, both non-photooxidized and photooxidized secondary NPLs were successfully produced using a highly efficient method, yielding 0.199 mg of secondary NP-PBAT-NPLs per gram of PBAT-microbeads These yields are comparable to those reported in previous studies ranging from 0.09 to 0.25 mg/g of NPLs below 100 nm[30]. The capability to produce sufficient quantities of NPLs, particularly those other than PS, is crucial for advancing toxicity testing and might be useful for developing standardized protocols for NPLs detection in real samples. Moreover, this method enables the production of dry PBAT-NPLs and PBAT-Olig, allowing for storage and subsequent resuspension at the desired concentration in any testing culture media. This contrasts with other methods where NPLs are resuspended in water, which subjects them to hydrolytic degradation during the process, complicating storage[29,30]. Additionally, our method avoids the use of surfactants to maintain particle dispersion replacing it by ethanol as suggested by the programme NANoREG for a common European approach to the regulatory testing of nanomaterials[54]. This is significant as surfactants can influence ecotoxicological assessments[55]. Despite the absence of surfactants, stable NPLs suspensions

were achieved, as evidenced by a ζ-potential of less than -30 mV. The hydrodynamic sizes of PBAT-NPLs was <70 nm, which is smaller than those reported in previous studies for instance using cryomilling and highly relevant especially in the phytotoxicology field considering recent outcomes regarding the microalgal differential uptake for NPLs < 100 nm[56,57]. Thus, a key advantage of the method presented here is that it generates NPLs without the need of prior photooxidation, unlike other techniques that rely on photodegradation processes.

The oligomeric fraction was also efficiently produced and isolated with a yield of 10.275 mg of NP-PBAT-Olig per gram of PBAT-microbeads. Olig have been defined based on degree of polymerization (< 40 units) or the molecular weight (< 10 kDa) and they have been detected during washing of polyester textiles[58]. However, these oligomers (with a mean size of 94-170 nm) fall within the size range that were classify as NPLs in this study, due to their hydrophobic-driven self-aggregation in aqueous media. These sizes might vary depending on the surrounding environment and therefore, they may behave as individual molecules in contact with biological membranes[10]. In our previous research, Olig were defined as molecules < 50 kDa, in which yields reaching up to 3.17 mg of PCL-Olig per gram of PCL-microbeads after 132 days under hydrolytic and non-UV photodegradation conditions in water were obtained[8]. The method presented here is faster and enables the production of purified isolated oligomers without photodegradation. Analysis of the oligomeric fraction by FTIR indicates the presence of characteristic C=O stretch peak. The difference between NPLs and the oligomers is the combination, in the case of the oligomer, of the 1732 cm^{-1} and 1720 cm^{-1} peaks (corresponding to the C=O stretching vibration in the amorphous and crystalline region of the polymer, respectively) in one single peak. The combination of this peak has been reported in other semicrystalline biodegradable polymers like poly(ϵ-caprolactone) as a consequence of the loss of solid status, where crystalline and amorphous regions are lacking[59]. Furthermore, for the ecotoxicology field, a novel characterization approach was employed, involving the separation of the oligomeric chains by polarity-dependent on hydrocarbon chain length and monomer composition, specifically the presence of butylene-terephthalate units (as shown in Fig S2. and Fig S3.). This was followed by individual MALDI-TOF/TOF analysis of each separated peak, preventing low-mass saturation of the detector[60]. The applied approach allowed us to precisely identify both linear and cyclic oligomers, including their formula, structures, and number of repeating units. Thus, this approach allowed the comparison between the oligomeric length, which was shorter for the P-PBAT oligomer compared to the non-photooxidized ones and indicated the potentially higher abundance of the smallest oligomers, such as cyclic dimers or trimers, as a result of the photooxidation exposure, being this fraction the most abundant in both samples. This detailed characterization is significant as it provides exact information on the oligomeric composition, enabling the testing of specific oligomer fractions separately. While some studies have highlighted the effects of certain biodegradable and non-biodegradable plastics derived oligomers[10,61,62], the structures and fundamental properties of oligomers generated from most polymers are still poorly understood. Despite their potential ubiquity[63], to date, secondary oligomers generated from plastics have been overlooked or poorly investigated, without acquiring this critical compositional information[64], which, however, has been partially obtained for those present in non-degraded plastics together with additives and other leachates[42].

The present study provides novel evidence on the impact of secondary NPLs generated from a biodegradable plastic such as PBAT on freshwater primary producers; although there are several studies of the effect of NPLs on these organisms, fundamentally cyanobacteria and green algae, they have been mostly done using primary NPLs, basically polystyrene ones with a specific size and shape (usually spherical) and for these reasons, their environmental relevance is unclear[65–74]. When using as toxicity endpoints general parameters such as growth and chlorophyll content, there were no significant differences between the effect of photooxidized and non-phootoxidized NPLs (p values were 0.170 and 0.278 for the lowest and the highest concentrations, respectively); however, a slight difference in ROS production values was observed for NP and P-PBAT-NPLs mainly at the lowest and higher concentrations tested of 0.01 and 50 mg/L respectively. These differences were not significant ($p > 0.05$) between photooxidized and non-photooxidized NPLs treatments and could be due to the slightly higher ζ-potential of the non-protoxidized NPLs that may preserve a more dispersed colloidal suspension, increasing bioavailability and consequently the observed trend to provoke higher toxicity. Furthermore, photooxidized NPLs tend to be more unstable when co-exposed together with organic matter and divalent ions that were present in the culture medium (Ca^{2+} and Mg^{2+}), thus, in addition of the presence of exopolysaccharide and other organic substances released by the cells could decrease P-PBAT-NPLs stability and therefore their bioavailability explaining the differences

seen in ROS overproduction between photooxidized and non-photooxidized NPLs[75]. Regarding mechanisms of toxic actions on the green alga, PBAT-NPLs, both photooxidized and non-photooxidized, induced ROS overproduction in the alga at the lowest concentrations tested (e.g., 0.01 mg/L and 1 mg/L), which are environmentally relevant since concentrations up to 1,588 µg/L have been quantified in a Swedish lake meaning that these NPLs might pose a threat to primary producers in freshwaters[17]. Besides, the estimated increase of fragmentation of larger plastic fractions in the environment might result in the number of NPs in natural ecosystem being possibly even much higher than that of microplastics[47]. An increase in the level of ROS is a common initial response to NPLs in primary producers such as algae and cyanobacteria[7,8,67,68,72–74]. The observed increase in ROS levels is consistent with the lipid peroxidation and concomitant membrane integrity damage and is also consistent with photosynthetic activity inhibition as reported in previous works[7,72,76,77]. In the long term, even when algal cells are exposed to low NPLs concentrations, a sustained oxidative damage, particularly if cells are unable to restore the balance between ROS and antioxidant defences, as a result of NPL exposure may increase membrane disruption increasing non-specific ion permeability[7,8,68,69,72] and lead to a continued damage of the photosynthetic machinery, consistent with the known effects of ROS on photosynthesis [65,67–69,72,73]. Despite the moderate knowledge concerning plastic oligomers considered as non-intentionally added substances (NIAS) in food contact materials, little is known about their impact on the environment[45,64]. The chemical formation of oligomers occurs during the polymerization process, either as a result of incomplete polymerization or due to thermal or hydrolytic degradation of polymer chains during the processing of the polymeric material or under conditions of use. The resulting oligomer profile can be highly complex, consisting of linear, branched, and cyclic species, each of which may exhibit different migration behaviour[78]. Due to the current awareness about the massive entrance of plastic wastes into the environment, it is crucial to understand the processes driving their release as well as their ecotoxicity. The release under environmental soft conditions as well as the lower toxicity of the oligomeric fraction compared to the nanoparticulate fraction have been previously observed for secondary polycaprolactone (PCL) oligomers and NPLs assessed in two cyanobacteria. The higher toxicity exerted by the PCL-NPLs has been related to the physical abrasion that the particles may cause in comparison to the oligomers, a hypothesis supported by a greater cytoplasmic membrane depolarization caused by the PCL-NPLs in comparison to the PCL-Olig. Consistently, the results obtained in the present study show a higher toxicity of the nanoparticulate fraction, supported by a cytoplasmic membrane depolarization and ROS overproduction, at lower concentrations with respect to the effect provoked by the oligomeric fraction. Interestingly, the observed decrease in photosynthetic activity, as measured by oxygen evolution, revealed a similar toxicity by both NPLs and oligomeric fractions, which could be due to the potential capability of the oligomers to cross the cytoplasmic membranes, due to their hydrophobic nature, endangering the photosynthetic function[62]. In this regard, a similar alteration caused by both fractions was observed on nitrogen fixation in a cyanobacterium exposed to secondary PCL NPLs and PCL oligomers[8]. The results presented in this study point towards a long-term impact of secondary NPLs and Olig on freshwater primary producers and possibly other components of the aquatic trophic chain that merits further research. The study also emphasizes the need to develop protocols for generating sufficient quantities of reference NPLs of each polymer, including biodegradable polymers, as they both may pose future environmental concerns. Additionally, it underscores the importance of investigating the generation of Olig and their impact on biota.

5. Conclusions

In this work, an improved method for the production of secondary nanoplastics (NPLs) and oligomers by simulating different processes of abiotic degradation in controlled conditions has been proposed that may be useful for the generation of reference NPLs in sufficient quantities to study their impact on biota. The generation and characterization of generated oligomers might be also extremely useful to further characterize the complete fragmentation of larger plastic fraction in the environment and also assess their environmental impact. This method has been applied successfully for the generation of secondary photooxidized and non-photooxidized PBAT-NPLs and PBAT-Olig materials that have been utilized to test multiple ecotoxicological parameters in the green alga *C. reinhardtii* showing an increased ROS overproduction that results in cytoplasmic membrane impairment and photosynthesis inhibition that may be detrimental in the long-term even at realistic environmental concentrations which may further compromise the aquatic trophic chain. This study encourages the development of protocols to generate reference NPLs of a variety of polymers including biodegradable polymers as they might not be entirely safe for the environment and the need to study the

environmental impact of oligomers

Acknowledgements

The authors acknowledge the financial support provided by the Spanish Government, Ministry of Science Grants TED2021-131609B-C32/33, PID2020-113769RB-C21/C22, PLEC2021-007693 and RyC2021-034953-I from the European Union NextGenerationEU/PRTR.

References

1. Plastics Europe ES. Plastics – the *fast* Facts 2023. Brussels.
2. Meijer LJJ, Van Emmerik T, Van Der Ent R, Schmidt C, Lebreton L. More than 1000 rivers 730 account for 80 % of global riverine plastic emissions into the ocean. Sci. Adv. 2021; 7(18):eaaz5803.
3. Lebreton LCM, Van Der Zwet J, Damsteeg JW, Slat B, Andrady A, Reisser J. River plastic 733 emissions to the world's oceans. Nat. Commun. 2017; 8(1):15611.
4. Zhang K, Hamidian AH, Tubić A, Zhang Y, Fang JKH, Wu C, Lam PKS. Understanding plastic degradation and microplastic formation in the environment: A review. Environ. Pollut. 2021;274:116554.
5. Song YK, Hong SH, Eo S, Shim WJ. The fragmentation of nano- and microplastic particles from thermoplastics accelerated by simulated-sunlight-mediated photooxidation. Environ. Pollut. 2022; 311:119847.
6. Erickson HP. Size and shape of protein molecules at the nanometer level determined by sedimentation, gel filtration, and electron microscopy. Biol. Proced. Online 2009; 11(1):32–51.
7. González-Pleiter M, Tamayo-Belda M, Pulido-Reyes G, Amariei G, Leganés F, Rosal R, Fernández-Piñas F. Secondary nanoplastics released from a biodegradable microplastic severely impact 745 freshwater environments. Environ. Sci. Nano. 2019; 6(5):1382–92.
8. Tamayo-Belda M, Pulido-Reyes G, González-Pleiter M, Martín-Betancor K, Leganés F, Rosal R, Fernández-Piñas F. Identification and toxicity towards aquatic primary producers of the smallest fractions released from hydrolytic degradation of polycaprolactone microplastics. Chemosphere. 2022; 303:134966.
9. Serrano-Lotina A, Portela R, Baeza P, Alcolea-Rodriguez V, Villarroel M, Ávila P. Zeta potential as a tool for functional materials development. Catalysis Today. 2023; 423:113862.
10. Wang M, Li Q, Shi C, Lv J, Xu Y, Yang J, Chua SL, Jia L, Chen H, Liu Q, Huang C, Huang Y, Chen J, Fang M. Oligomer nanoparticle release from polylactic acid plastics catalysed by gut enzymes triggers acute inflammation. Nat. Nanotechnol. 2023; 18(4):403-411.
11. Hernandez LM, Yousefi N, Tufenkji N. Are there nanoplastics in your personal care products? Environ. Sci. Technol. Lett. 2017; 4(7):280–5.
12. Cai H, Xu EG, Du F, Li R, Liu J, Shi H. Analysis of environmental nanoplastics: Progress and 760 challenges. Chem. Eng. J. 2021; 410:128208.
13. Mandemaker LDB, Meirer F. Spectromicroscopic techniques for studying nanoplastics in the environment and in organisms. Angew. Chem. 2023; 135:e202210494.
14. Kau D, Materić D, Holzinger R, Baumann-Stanzer K, Schauer G, Kasper-Giebl A. Fine micro-and nanoplastics concentrations in particulate matter samples from the high alpine site Sonnblick, Austria. Chemosphere 2024; 352:141410.
15. Materić D, Kjær HA, Vallelonga P, Tison JL, Röckmann T, Holzinger R. Nanoplastics measurements in Northern and Southern polar ice. Environ. Res. 2022; 208:112741.
16. Materić D, Holzinger R, Niemann H. Nanoplastics and ultrafine microplastic in the Dutch Wadden Sea – The hidden plastics debris? Sci. Total Environ. 2022; 846:157371.
17. Materić D, Peacock M, Dean J, Futter M, Maximov T, Moldan F, Röckmann T, Holzinger R. Presence of nanoplastics in rural and remote surface waters. Environ Res Lett. 2022; 17(5):054036.
18. Materić D, Ludewig E, Brunner D, Röckmann T, Holzinger R. Nanoplastics transport to the remote, high-altitude Alps. Environ. Pollut. 2021; 288:117697.
19. Materić D, Kasper-Giebl A, Kau D, Anten M, Greilinger M, Ludewig E, van Sebille E, Röckmann T, Holzinger R.. Micro- and nanoplastics in alpine snow: A new method for chemical identification and (semi)quantification in the nanogram range. Environ. Sci. Technol. 2020; 54(4):2353.
20. Li Q, Lai Y, Li P, Liu X, Yao Z, Liu J, Yu S. Evaluating the occurrence of polystyrene nanoparticles in environmental waters by agglomeration with alkylated ferroferric oxide followed by micropore membrane filtration collection and Py-GC/MS analysis. Environ. Sci. Technol. 2022; 56(12):8255.
21. Xu Y, Ou Q, Jiao M, Liu G, Van Der Hoek JP. Identification and quantification of nanoplastics

in surface water and groundwater by pyrolysis gas chromatography–mass spectrometry. Environ. Sci. Technol. 2022; 56(8):4988–97.
22. Xu Y, Ou Q, Wang X, Hou F, Li P, Van Der Hoek JP, Liu G. Assessing the mass concentration of microplastics and nanoplastics in wastewater treatment plants by pyrolysis gas chromatography–mass spectrometry. Environ Sci Technol. 2023; 57(8):3114–23.
23. Chamas A, Moon H, Zheng J, Qiu Y, Tabassum T, Jang JH, Abu-Omar M, Scott SL, Suh S. Degradation rates of plastics in the environment. ACS Sust. Chem. Eng. 2020; 8(9):3494–511.
24. Venâncio C, Melnic I, Tamayo-Belda M, Oliveira M, Martins MA, Lopes I. Polymethylmethacrylate nanoplastics can cause developmental malformations in early life stages of *Xenopus laevis*. Sci. Total Environ. 2022; 806:150491.
25. Santos A, Oliveira M, Lopes I, Almeida M, Venâncio C. Polyhydroxybutyrate (PHB) nanoparticles modulate metals toxicity in *Hydra viridissima*. Sci. Total Environ. 2024; 932:172868.
26. Vicentini DS, Nogueira DJ, Melegari SP, Arl M, Köerich JS, Cruz L, Justino NM, Oscar BV, Puerari RC, da Silva MLN, Simioni C, Ouriques LC, Matias MS, de Castilhos-Junior AB, Matias WG. Toxicological evaluation and quantification of ingested metal-core nanoplastic by *Daphnia magna* through fluorescence and inductively coupled plasma-mass spectrometric methods. Environ. Toxicol. Chem. 2019; 38(10):2101–10.
27. Mitrano DM, Beltzung A, Frehland S, Schmiedgruber M, Cingolani A, Schmidt F. Synthesis of metal-doped nanoplastics and their utility to investigate fate and behaviour in complex environmental systems. Nat. Nanotechnol. 2019; 14(4):362–8.
28. Peller JR, Mezyk SP, Shidler S, Castleman J, Kaiser S, Faulkner RF, Pilgrim CD, Wilson A, Martens S, Horne GP. Facile nanoplastics formation from macro and microplastics in aqueous media. Environ. Pollut. 2022; 313:120171.
29. Merdy P, Delpy F, Bonneau A, Villain S, Iordachescu L, Vollertsen J, Lucas Y. Nanoplastic 809 production procedure for scientific purposes: PP, PVC, PE-LD, PE-HD, and PS. Heliyon 2023; 9(8):e18387.
30. Ji Y, Wang C, Wang Y, Fu L, Man M, Chen L. Realistic polyethylene terephthalate nanoplastics and the size- and surface coating-dependent toxicological impacts on zebrafish embryos. Environ. Sci. Nano 2020; 7(8):2313–24.
31. Ekvall MT, Lundqvist M, Kelpsiene E, Šileikis E, Gunnarsson SB, Cedervall T. Nanoplastics formed during the mechanical breakdown of daily-use polystyrene products. Nanoscale Adv. 2019; 1(3):1055–61.
32. Tamayo-Belda M, Venâncio C, Fernandez-Piñas F, Rosal R, Lopes I, Oliveira M. Effects of petroleum-based and biopolymer-based nanoplastics on aquatic organisms: A case study with mechanically degraded pristine polymers. Sci. Total Environ. 2023; 883:163447.
33. Magrì D, Sánchez-Moreno P, Caputo G, Gatto F, Veronesi M, Bardi G, Catelani T, Guarnieri D, Athanassiou A, Pompa PP, Fragouli D. Laser ablation as a versatile tool to mimic polyethylene terephthalate nanoplastic pollutants: Characterization and toxicology Assessment. ACS Nano. 2018; 12(8):7690–700.
34. Ji Y, Chen L, Wang Y, Zhang J, Yu Y, Wang M, Wang X, Liu W, Yan B, Xiao L, Song X, Lv C, Chen L. Realistic Nanoplastics induced pulmonary damage via the crosstalk of ferritinophagy and mitochondrial dysfunction. ACS Nano. 2024; 18(26):16790–807.
35. Tamayo-Belda M, Pulido-Reyes G, Rosal R, Fernández-Piñas F. Nanoplastic toxicity towards freshwater organisms. Water Emerg Contam & Nanoplastics. 2022; 1(4):19.
36. McConnel G, Kasuske ZA, Mazariegos-Ortíz C, Muñoz SR, Cañas-Carrell JE. A systems perspective of terrestrial, aquatic, and human health impacts of non-polystyrene-based nanoplastics. Curr. Opin. Environ. Sci. Health 2024; 39:100557.
37. Khan A, Jia Z. Recent insights into uptake, toxicity, and molecular targets of microplastics and nanoplastics relevant to human health impacts. iScience. 2023; 26(2):106061.
38. Kauts S, Shabir S, Yousuf S, Mishra Y, Bhardwaj R, Milibari AA, Singh SK, Singh MP. The evidence of in-vivo and in-vitro studies on microplastic and nano plastic toxicity in mammals: A possible threat for an upcoming generation? PPhys. Chem. Earth. A/B/C 2023; 132:103511.
39. Subramanian D, Ponnusamy Manogaran G, Dharmadurai D. A systematic review on the impact of micro-nanoplastics on human health: Potential modulation of epigenetic mechanisms and identification of biomarkers. Chemosphere. 2024; 363:142986.
40. Bai CL, Wang D, Luan YL, Huang SN, Liu LY, Guo Y. A review on micro- and nanoplastics in humans: Implication for their translocation of barriers and potential health effects. Chemosphere 2024; 361:142424.
41. Casella C, Ballaz SJ. Genotoxic and neurotoxic potential of intracellular nanoplastics: A review.

J. Appl. Toxicol. 2024; 44(11):1657.

42. Zimmermann L, Dombrowski A, Völker C, Wagner M. Are bioplastics and plant-based materials safer than conventional plastics? In vitro toxicity and chemical composition. Environ. Int. 2020; 145:106066.
43. Pinaeva LG, Noskov AS. Biodegradable biopolymers: Real impact to environment pollution. Sci. Total Environ. 2024; 947:174445.
44. Qin M, Chen C, Song B, Shen M, Cao W, Yang H, Zeng G, Gong J. A review of biodegradable plastics to biodegradable microplastics: Another ecological threat to soil environments? J. Cleaner Prod. 2021; 312:127816.
45. Hoppe M, De Voogt P, Franz R. Identification and quantification of oligomers as potential migrants in plastics food contact materials with a focus in polycondensates – A review. Abbreviation Title Trends Food Sci. Technol. 2016; 50:118.
46. Zarna C, Rodríguez-Fabià S, Echtermeyer AT, Chinga-Carrasco G. Preparation and characterisation of biocomposites containing thermomechanical pulp fibres, poly(lactic acid) and poly(butylene-adipate-terephthalate) or poly(hydroxyalkanoates) for 3D and 4D printing. Addit. Manuf. 2022; 59:103166.
47. Sorasan C, Edo C, González-Pleiter M, Fernández-Piñas F, Leganés F, Rodríguez A, Rosal R. Generation of nanoplastics during the photoageing of low-density polyethylene. Environ. Pollut. 2021; 289: 117919.
48. Hurtado-Gallego J, Pulido-Reyes G, González-Pleiter M, Salas G, Leganés F, Rosal R, Fernández-Piñas F. Toxicity of superparamagnetic iron oxide nanoparticles to the microalga *Chlamydomonas reinhardtii*. Chemosphere. 2020; 238:124562.
49. Jeffrey SW, Humphrey GF. New spectrophotometric equations for determining chlorophylls *a*, *b*, c_1 and c_2 in higher plants, algae and natural phytoplankton. Biochemie und Physiologie der Pflanzen 1975; 167(2):191.
50. Tamayo-Belda M, González-Pleiter M, Pulido-Reyes G, Martin-Betancor K, Leganés F, Rosal R, Fernández-Piñas F. Mechanism of the toxic action of cationic G5 and G7 PAMAM dendrimers in the cyanobacterium: Anabaena sp. PCC7120. Environ. Sci. Nano 2019; 6(3):863.
51. Ortega-Villasante C, Rellán-Álvarez R, Del Campo FF, Carpena-Ruiz RO, Hernández LE. Cellular damage induced by cadmium and mercury in *Medicago sativa*. J . Exp. Bot. 2005; 56(418):2239.
52. Leganés F, Martínez-Granero F, Muñoz-Martín MÁ, Marco E, Jorge A, Carvajal L, Vida T, González-Pleiter M, Fernández-Piñas F. Characterization and responses to environmental cues of a photosynthetic antenna-deficient mutant of the filamentous cyanobacterium Anabaena sp. PCC 7120. J. Plant Physiol. 2014; 171(11):915–26.
53. de Matos Costa AR, Crocitti A, Hecker de Carvalho L, Carroccio SC, Cerruti P, Santagata G. Properties of biodegradable films based on poly(butylene succinate) (PBS) and poly(butylene adipate-co-terephthalate) (PBAT) blends. Polymers 2020; 12(10):2317.
54. Booth A, Jensen K. Protocol for producing reproducible dispersions of manufactured nanomaterials in environmental exposure media Preparation and physicochemical characterisation of manufactured nanomaterials (MNMs) in environmental fate and ecotoxicity exposure media." Dispersion Standard Operating Procedure 2015.
55. Pikuda O, Xu EG, Berk D, Tufenkji N. Toxicity assessments of micro- and nanoplastics can be confounded by preservatives in commercial formulations. Environ Sci Technol Lett. 2019; 6(1):21–5.
56. McColley CJ, Nason JA, Harper BJ, Harper SL. An assessment of methods used for the generation and characterization of cryomilled polystyrene micro- and nanoplastic particles. Microplast. Nanoplast. 2023; 3(1):20.
57. Wang Y, Yan N, Ji Q, Chen S, Huang Y, Wong TY, Hu Y, Shi J. Novel insights into the joint phytotoxicity of environmental relevant concentration nanoplastics and silver ions: A dual aggregation-induced emission bioimaging approach. Environ. Sci. Nano 2024, 11: 4521.
58. Yang T, Xu Y, Liu G, Nowack B. Oligomers are a major fraction of the submicrometre particles released during washing of polyester textiles. Nat Water. 2024; 2(2):151.
59. Phillipson K, Hay JN, Jenkins MJ. Thermal analysis FTIR spectroscopy of poly(ϵ-caprolactone). Thermochim. Acta. 2014; 595:74–82.
60. Westman A, Brinkmalm G, Barofsky DF. MALDI induced saturation effects in chevron microchannel plate detectors. Int. J. Mass Spectrom. Ion Processes 1997; 169–170:79.
61. Yoshinaga N, Tateishi A, Kobayashi Y, Kubo T, Miyakawa H, Satoh K, Numata K. Effect of Oligomers derived from biodegradable polyesters on eco- and neurotoxicity. Biomacromolecules 2023; 24(6):2721.
62. Järvenpää J, Perkkiö M, Laitinen R, Lahtela-Kakkonen M. PE and PET oligomers' interplay with membrane bilayers. Sci Rep. 2022;

12(1):2234.
63. Kwon BG, Koizumi K, Chung SY, Kodera Y, Kim JO, Saido K. Global styrene oligomers monitoring as new chemical contamination from polystyrene plastic marine pollution. J. Hazard. Mater. 2015 ;300:359.
64. Shi C, Wang M, Wang Z, Qu G, Jiang W, Pan X, Fang M. Oligomers from the synthetic polymers: another potential iceberg of new pollutants. Environ Health 2023; 1(4):228.
65. Li X, Qiu H, Zhang P, Song L, Romero-Freire A, He E. Role of heteroaggregation and internalization in the toxicity of differently sized and charged plastic nanoparticles to freshwater microalgae. Environ. Pollut. 2023; 316:120517.
66. Déniel M, Lagarde F, Caruso A, Errien N. Infrared spectroscopy as a tool to monitor interactions between nanoplastics and microalgae. Anal Bioanal Chem. 2020; 412(18):4413.
67. Yang W, Gao P, Nie Y, Huang J, Wu Y, Wan L, Ding H, Zhang W. Comparison of the effects of continuous and accumulative exposure to nanoplastics on microalga *Chlorella pyrenoidosa* during chronic toxicity. Sci. Total Environ. 2021; 788:147934.
68. Yang W, Gao P, Ma G, Huang J, Wu Y, Wan L, Ding H, Zhang W. Transcriptome analysis of the toxic mechanism of nanoplastics on growth, photosynthesis and oxidative stress of microalga *Chlorella pyrenoidosa* during chronic exposure. Environ. Pollut. 2021; 284:117413.
69. Wang S, Liu M, Wang J, Huang J, Wang J. Polystyrene nanoplastics cause growth inhibition, morphological damage and physiological disturbance in the marine microalga *Platymonas helgolandica*. Mar. Pollut. Bull. 2020; 158:111403.
70. Reynolds A, Giltrap DM, Chambers PG. Acute growth inhibition & toxicity analysis of nanopolystyrene spheres on *Raphidocelis subcapitata*. Ecotox. Environ. Saf. 2021; 207:111153.
71. Yang Y, Guo Y, O'Brien AM, Lins TF, Rochman CM, Sinton D. Biological responses to climate change and nanoplastics are altered in concert: Full-factor screening reveals effects of multiple stressors on primary producers. Environ Sci Technol. 2020; 54(4):2401.
72. Tamayo-Belda M, José Vargas-Guerrero J, Martín-Betancor K, Pulido-Reyes G, González-Pleiter M, Leganés F, Rosañ R, Fernández-Piñas F. Understanding nanoplastic toxicity and their interaction with engineered cationic nanopolymers in microalgae by physiological and proteomic approaches. Environ. Sci. Nano 2021; 8(8):2277.
73. Zheng X, Yuan Y, Li Y, Liu X, Wang X, Fan Z. Polystyrene nanoplastics affect growth and microcystin production of *Microcystis aeruginosa*. Environ. Sci. Pollut. Res. 2021; 28(11):13394.
74. Xin X, Chen B, Péquin B, Song P, Yang M, Song X, et al. Binary toxicity of polystyrene nanoplastics and polybrominated diphenyl ethers to arctic cyanobacteria under ambient and future climates. Water Res. 2022; 226:119188.
75. Lian F, Han Y, Zhang Y, Li J, Sun B, Geng Z, Wang Z. Exposure order to photoaging and humic acids significantly modifies the aggregation and transformation of nanoplastics in aqueous solutions. Environ. Sci. Technol. 2023; 57(16):6520.
76. Latifi A, Ruiz M, Zhang CC. Oxidative stress in cyanobacteria. FEMS Microbiol. Rev. 2009; 33(2):258.
77. Verdú I, González-Pleiter M, Leganés F, Fernández-Piñas F, Rosal R. Leaching of herbicides mixtures from pre-exposed agricultural plastics severely impact microalgae. Chemosphere 2023; 326:138475.
78. Schaefer A, Ohm VA, Simat TJ. Migration from can coatings: Part 2. Identification and 954 quantification of migrating cyclic oligoesters below 1000 Da. Food Addit. Contam. 2004; 21(4):377.

Supplementary Information

An Improved method to generate secondary nanoplastics and oligomers: Application in ecotoxicology

Silvia Gómez-Kong[1], Miguel Tamayo-Belda[1], Gerardo Pulido-Reyes[1], Carlos Edo[2], Irene Verdú[1], Francisco Leganés[1,3], Roberto Rosal[2], Miguel González-Pleiter[1,3], Francisca Fernández-Piñas[1,3,*]

[1]Department of Biology, Faculty of Science, Universidad Autónoma de Madrid, E-28049, Madrid, Spain
[2]Department of Chemical Engineering, Universidad de Alcalá, E-28871 Alcalá de Henares, Madrid, Spain
[5]Centro de Investigación en Biodiversidad y Cambio Global (CIBC-UAM), Universidad Autónoma de Madrid. Darwin 2, 28049 Madrid, Spain

* Corresponding author: francisca.pina@uam.es

Contents:

NP/P-PBAT-NPLs & NP/PPBAT-Olig. **Table S9**. Raw data cell size based on flow cytometry back scatter detected with forward scatter FSC of *C. reinhardtii* cells after 72 h exposure to NP/PPBAT-NPLs & NP/P-PBAT-Olig. **Figure S1**. Size Distribution curves by number of NP- and P-PBATNPLs and NP- and P-PBAT-Olig in ultrapure water (A). Size Distribution curves by number of NP- and P-PBAT-NPLs and NP- and P-PBAT-Olig in culture medium (B).

Figure S2. MALDI-TOF/TOF spectrum of NP-PBAT-Olig chromatography peaks 1(A), 2(B), 3(C), 4(D), 5(E), 6(F), 7(G) and 8 (H).

Figure S3. MALDI-TOF/TOF spectrum of P-PBAT-Olig chromatography peaks 1(A) 2(B), 3(C), 4(D), 5(E) and 6(F).

Figure S4. Mean value of butylene-terephthalate units per polymeric series by chromatography peak (from lower to higher hydrophobicity) of NP- (A) and P- (B) PBAT-Olig.

Figure S5. Growth, expressed as percentage of variation of OD_{750}, on *C. reinhardtii* after 72 h exposure to NP/P-PBAT-NPLs & NP/P-PBAT-Olig. Asterisks indicate treatments that are significantly different (Dunnet's test, (***) $p < 0.001$, (**) $p < 0.01$, (*) $p < 0.05$) from the control represented as 100 % (dotted line).

Figure S6. Chlorophyll content expressed as percentage of variation of total chlorophylls on *C. reinhardtii* after 72 h exposure to NP/P-PBAT-NPLs & NP/PPBAT-Olig. Asterisks indicate treatments that are significantly different (Dunnet's test, (***) $p < 0.001$, (**) $p < 0.01$, (*) $p < 0.05$) from the control represented as 100 % (dotted line).

Figure S7. Representative chlorophyll autofluorescence/bright field overlay images of confocal microscopy of *C. reinhardtii* after 72 h exposure to NP- and P-PBAT-NPLs. Image shows confocal microscopy images of the non-exposed cells (A and D); cells exposed to 0.1 and 10 mg/L of NP-PBAT-NPLs (B and C, respectively); cells exposed to 0.1 and 10 mg/L of P-PBAT-NPLs (E and F, respectively).

Supplementary Text 1. Protocol to generate, isolate and quantify nanoplastics (NPLs) and oligomers (Olig) through accelerated degradation processes: trituration (nonphotooxidized (NP)-NPLs) and photooxidation followed by trituration (photooxidized (P)-NPLs).

1 Materials and equipment

◦ Stainless-steel blender (Figure Supplementary Text 1).

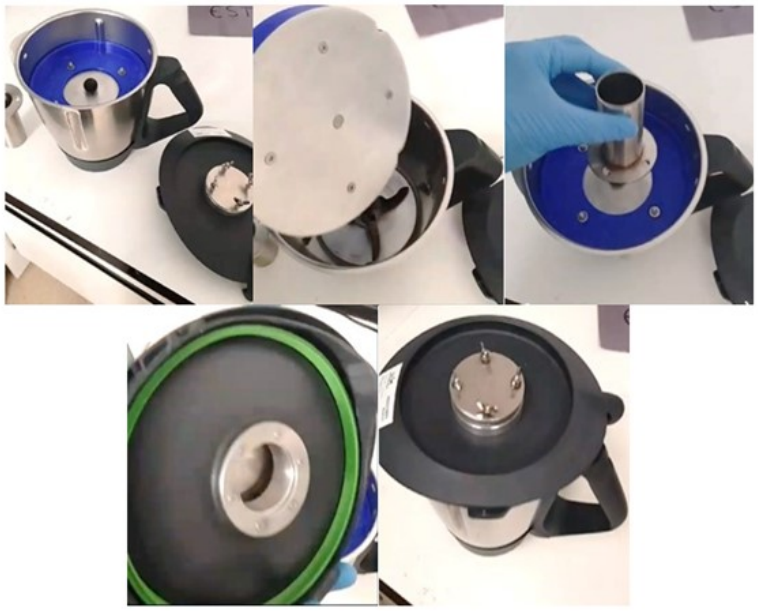

Figure ST1: *Pictures of the modified stainless-steel blender Thermomix TM31 (Vonwerk, Germany) used for the protocol.*

◦ High power ultraviolet lamp (Figure Supplementary Text 2).

Figure ST2: *9.34 kW m^{-2} at 4 cm medium-pressure mercury lamp (Novalight TQ150) used for the protocol.*

◦ 1mm pore metal strainer with a metal bowl or collector underneath to collect material passing through the filter.
◦ Liquid nitrogen.
◦ Magnetic stirrer and magnet.
◦ 50 kDa (50,000 Daltons) MWCO (Molecular Weight Cut-Off) ultrafiltration tubes.
◦ Ultra-pure ethanol (> 99.5 %).

◦ 50 mL Falcon tubes.
◦ Tip sonicator.
◦ 1 µm pore filter suitable for large volumes.
◦ Drying oven that reaches 60°C.
◦ Beaker glasses.
◦ Precision balance (capable of weighing up to 0.01 mg).
◦ Empty glass vials suitable for precision scales (number the glass vial with an indelible marker before weighing and do not erase).

Each generation process requires the use of ultrafiltration tubes, which must be cleaned before use as follows (Section 1.1):

a) Take 4 ultrafiltration tubes with a capacity of 20 ml in the upper part.
b) Add 20 ml of ultrapure water and centrifuge them for 2 min at 4500 rcf.
c) Discard the filtered volume remaining in the lower part.
d) Repeat steps b) and c) 3 more times until washing the 4 tubes have been washed 4 times with ultrapure water.

2 Obtention of non-photooxidized nanoplastics and oligomers by trituration

2.1 Material trituration process. Triturate up to 300 g of microbeads in the stainless-steel blender to obtain 210 g (70 % of the original material) of triturated material < 1 mm.

a) Place the microbeads to be triturated in a metal or resistant plastic (polypropylene) container.
b) Fill the container with liquid nitrogen until the microbeads are covered and let it evaporate.
c) Allow the microbeads to heat up at room temperature for 1-2 minutes before triturating (if the surface of the microbeads is too cold, the blender is likely to block).
d) Add the microbeads in the blender and triturate for 1-2 min at maximum revolutions (10,000 rpm). Be careful, the material will continue to heat up during the trituration process, stop the process if the temperature exceeds 30 degrees and continue with step e).
e) Once triturated, transfer the material from the blender to the 1 mm pore strainer and shake until all the material < 1 mm passes into the collector.
f) Transfer the fragmented microbeads (> 1 mm) directly from the strainer and repeat steps a), b), c), d) and f) until an approximate amount of 30 % wt of the original material remains in the strainer (this amount may vary depending on the polymer).At this point, the small amount and small size of the fragmented microbeads make the process too inefficient).
g) Store the grinded material < 1 mm in glass bottles, avoiding exposure to light (use amber bottle, cover the bottle with aluminum, store in an opaque cabinet...).

The NPLs and oligomers generated are mixed with the triturated material < 1 mm.

2.2 Isolation, purification and quantification (dry weight) of nanoplastics and oligomers generated by trituration. Based on the application of the protocol with PBAT, we estimate that this protocol will yield between 2 and 4 mg of NPLs per 20 g of triturated material < 1mm. This process is performed in two consecutive phases, the first aims to isolate the oligomeric fraction in ultra-pure ethanol, as the main objective, together with a small amount of the NPLs; the second phase is focused on extracting the maximum amount of NPLs using an ethanol/water mixture during the extraction. It is proposed to discard the volume retained in the lower part since it contains water, which would make the isolation of the oligomeric

fraction take a considerable amount of time (the oligomers are usually most of the mass fraction, whereby enough material would be obtained only with the Phase 1):

a) Start transferring 80 grams of triturated material (< 1 mm) [section 2.1)] to 4 100 mL beaker glasses (20 g per beaker glass).

Phase 1

b) Add 80 mL of ultra-pure ethanol at 30 °C to each beaker glass.
c) Sonicate each beaker glass individually for 1 min using a tip sonicator at enough power to shake the whole triturated material (typically at 60 % duty cycle and 260 W using a Branson Ultrasonics™ Sonifier™ S-450A) and allow the material to settle for 1 min.
d) Collect the maximum possible volume of ultra-pure ethanol (320 mL) and filter through a 1 µm pore filter.

It is important not to exceed the flow rate recommended by the manufacturer, which in the case of glass fiber filters (Whatman) is 81 mL/min, to avoid the release of glass microfibers into the samples. For greater safety, a stainless-steel filter with a 10 µm pore size can be placed between the glass fiber filter and the support (in contact with the filter) to retain the fibers that come off (most of which are larger than 10 µm) or use a nylon filter. For avoid the filter clogging, replace the filter every 100 mL.

e) Transfer the filtered material to the upper part of 4 ultrafiltration tubes (20 mL per tube).
f) Centrifuge the ultrafiltration tubes at room temperature at 4000 rcf until the entire volume is ultrafiltered (2-4 min).
g) The volume retained in the lower part of the tubes should be kept separately, it is the oligomeric fraction (Text S1 Fig. 3).
h) Repeat steps e), f) and g) until the entire volume (320 mL) is ultrafiltered.

The last centrifugations may take longer due to the membranes clogging (usually not more than 10 minutes).

i) After ultrafiltration of the entire volume, transfer the oligomeric fraction to a beaker glass and dry in a clean oven at 60 °C until complete drying (dried oligomers have an oily appearance).
j) Resuspend the material in 2-3 mL of ultra-pure ethanol and transfer it to an empty and previously weighed small glass vial (weigh without cap) and dry it in a clean oven at 60 °C until completely dry (dried oligomers present oily appearance).

Phase 2

k) Prepare 320 mL of 25 % v/v ultra-pure ethanol in ultra-pure water (240 mL of ultra-pure water and 80 mL of ultra-pure ethanol in a glass bottle).
l) Transfer 80 mL of the solution prepared in the previous step, into 4 beaker glasses containing 20 g of triturated material (< 1 mm) that has already been extracted with ultra-pure ethanol following Phase 1 (new triturated material can be added to increase the efficiency of NPLs extraction).
m) Cool the beaker glasses at 4 °C for 15 min to prevent the dissolution of NPLs.
n) Sonicate each beaker glass individually for 1 min using a tip sonicator at enough power to shake the whole triturated material (typically at 60 % duty cycle and 260 W using a Branson Ultrasonics™ Sonifier™ S-450A) and allow the material to settle for 1 min.
o) Collect the whole possible volume of ultra-pure ethanol at 25 % in ultrapure water (250-300 mL) and filter through a 1 µm pore filter.

p) Store the filtered material at 4 °C for 10-15 minutes to prevent the dissolution of NPLs.
q) Transfer the filtered material to the upper part of the 4 ultrafiltration tubes used in the Phase 1 (20 mL per tube).
r) Centrifuge the ultrafiltration tubes at room temperature at 4000 rcf until the entire volume is ultrafiltered (5-15 min).
s) The volume retained at the bottom of the tubes is discarded in case the triturated material used had been previously subjected to the Phase 1 (it contains few oligomers; Text S1 Fig. 3).
t) Repeat steps m), n), r), and s) until the entire volume (300 mL) is ultrafiltered.

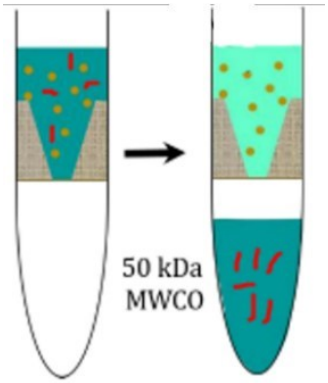

Figure ST3: *Graphical image of the ultrafiltration process (yellow circles represent nanoplastics, red lines oligomers less than 50 kDa).*

The last centrifugations may take longer due to the membranes clogging (usually not more than 10 minutes).

u) After ultrafiltering the entire volume, one more ultrafiltration should be performed using cold ultra-pure ethanol (1 h at 4 °C) to clean the fraction of NPLs that have been retained in the membranes.
v) The NPLs fraction is recovered by vigorously pipetting a volume of 2-3mL into the upper part of the tube, and subsequently that volume is stored in an empty and previously weighed small glass vial (weigh without cap) and dry it in a clean oven at 60 °C until completely dry.

2.3 Quantification by dry weight (for both, Phase 1 and Phase 2). When both fractions are dried, the small glass vials (without cap) containing the NPLs or the oligomers should be weighed. From this weight, the initial weight of the empty bottle (without cap) is subtracted to obtain the mass of the material generated. (Suggested balance accuracy ±0.01 mg.)

3 Obtention of photooxidized nanoplastics and oligomers by photooxidation followed by trituration

a) Place a maximum of 100 g of microbeads into the UV light lamp bottle filled with 800 mL of ultra-pure ethanol.
b) Allow the photo-aging test to run for the days defined in the experimental design on the basis of the power applied and the photoaging scenario to be simulated.

In this study the lamp irradiates at 9.34 kW m^{-2} (approximately 120 times the solar irradiance in the Iberian Peninsula) during 96 h, irradiation that corresponds to 16 months of average sunlight in the Iberian Peninsula (7.7 kWh m^{-2} day^{-1}).

c) Separately collect the ultra-pure ethanol (containing NPLs, oligomers and photooxidized

material > 1 µm) and the photooxidized microbeads.
d) Filter the ethanol from the previous step through 1 µm pore filters to isolate and purify the material contained in ultra-pure ethanol as follows:

d1). Transfer the filtered material to the upper part of 4 ultrafiltration tubes (20 mL per tube).
d2). Centrifuge the ultrafiltration tubes at room temperature at 4000 rcf until the entire volume is ultrafiltered (2-4 min).

The last centrifugations may take longer due to the membranes clogging (usually not more than 10 minutes).

d3). The volume retained in the lower part of the tubes should be kept separately, it is the oligomeric fraction (Text S1 Fig. 4).
d4). After storage of the photooxidized material, one more ultrafiltration should be performed using cold ultrapure ethanol (1 h at 4 °C) to clean the fraction of NPLs that have been retained in the membranes.
d5). The NPLs fraction is recovered by vigorously pipetting a volume of 2-3 mL into the upper part of the tube, and subsequently that volume is stored in an empty and previously weighed small glass vial (weigh without cap) and dry it in a clean oven at 60 °C until completely dry.

e) Triturate the photooxidized microbeads as described in section 2.2) and follow the Phase 1 and Phase 2 to obtain photooxidized nanoplastics and oligomers. Transfer these materials together with those obtained from the ultra-pure ethanol used during the photooxidation (described in section 3.d) to the same glass vials to proceed with the quantification by dry weight measurement (section 2.3).

Table S1. *pH of ultrapure water and culture medium with 50 mg/L of NP- and P-PBAT-Olig at 0 and 96 h.*

Medium	Ultrapure water		TAP/6)	
	0 h	96 h	0 h	96 h
Without Oligs	5.8	5.64	6.96	7.09
NP-PBAT-Olig	5.14	5.15	6.88	7.08
P-PBAT-Olig	4.47	4.54	6.85	7.08

Table S2. *Concentrations and incubation times of the fluorochrome probes used for flow cytometry.*

Fluorochrome	Acronym	Physiological parameter	Final concentration (µg mL^{-1})	Incubation time (min)	Channel
Dihydrorhodamine 123	DHR123	Intracellular levels of H_2O_2	10	40	FITC
Bis-(1,3-dibutylbarbituric acid) trimethine oxonol	$DiBAC_4(3)$	Cytoplasmic membrane potential	2.5	10	FITC

Table S3. *Raw data of C. reinhardtii growth measured as OD_{750} after 72 h exposure to NP/P-PBAT-NPLs & NP/P-PBAT-Olig.*

NP-PBAT-NPLs	OD_{750}, mean	OD_{750}, SD
Control for 0.01 mg/L	1.385	0.093
Control for 0.1 mg/L	1.090	0.049
Control for 1 mg/L	1.090	0.049
Control for 10 mg/L	1.090	0.049
Control for 50 mg/L	1.385	0.093
0.01 mg/L	1.262	0.058
0.1 mg/L	1.036	0.050
1 mg/L	1.019	0.076
10 mg/L	0.981	0.016
50 mg/L	1.248	0.101
P-PBAT-NPLs	OD_{750}, mean	OD_{750}, SD
Control for 0.01 mg/L	1.385	0.093
Control for 0.1 mg/L	1.385	0.093
Control for 1 mg/L	1.385	0.093
Control for 10 mg/L	1.385	0.093
Control for 50 mg/L	1.385	0.093
0.01 mg/L	1.171	0.033
0.1 mg/L	1.238	0.050
1 mg/L	1.275	0.074
10 mg/L	1.268	0.062
50 mg/L	1.263	0.142
NP-PBAT-Olig	OD_{750}, mean	OD_{750}, SD
Control for 0.01 mg/L	1.146	0.073
Control for 0.1 mg/L	1.125	0.072
Control for 1 mg/L	1.125	0.072
Control for 10 mg/L	1.125	0.072
Control for 50 mg/L	1.146	0.073
0.01 mg/L	1.188	0.100
0.1 mg/L	1.016	0.116
1 mg/L	1.160	0.136
10 mg/L	1.064	0.071
50 mg/L	0.975	0.091
P-PBAT-Olig	OD_{750}, mean	OD_{750}, SD
Control for 0.01 mg/L	1.146	0.073
Control for 0.1 mg/L	1.125	0.072
Control for 1 mg/L	1.125	0.072
Control for 10 mg/L	1.125	0.072
Control for 50 mg/L	1.146	0.073
0.01 mg/L	1.119	0.080
0.1 mg/L	1.142	0.134
1 mg/L	1.154	0.032
10 mg/L	1.108	0.062
50 mg/L	1.179	0.099

Table S4. *Raw data of C. reinhardtii chlorophyll content expressed as mg/L of total chlorophyll after 72 h exposure to NP/P-PBAT-NPLs & NP/P-PBATOlig.*

NP-PBAT-NPLs	Chlorophyl (*a*+*b*), mg/L, mean	Chlorophyl (*a*+*b*), mg/L, SD
Control for 0.01 mg/L	9.841	0.243
Control for 0.1 mg/L	7.379	0.145
Control for 1 mg/L	7.379	0.145
Control for 10 mg/L	7.379	0.145
Control for 50 mg/L	9.841	0.243
0.01 mg/L	9.741	0.269
0.1 mg/L	7.347	0.189
1 mg/L	6.823	0.851
10 mg/L	7.245	0.293
50 mg/L	9.732	0.556
P-PBAT-NPLs	Chlorophyl (*a*+*b*), mg/L, mean	Chlorophyl (*a*+*b*), mg/L, SD
Control for 0.01 mg/L	7.379	0.145
Control for 0.1 mg/L	7.379	0.145
Control for 1 mg/L	7.379	0.145
Control for 10 mg/L	7.379	0.145
Control for 50 mg/L	7.379	0.145
0.01 mg/L	10.374	0.689
0.1 mg/L	10.306	0.116
1 mg/L	10.441	0.017
10 mg/L	10.171	0.146
50 mg/L	9.461	1.362
NP-PBAT-Olig	Chlorophyl (*a*+*b*), mg/L, mean	Chlorophyl (*a*+*b*), mg/L, SD
Control for 0.01 mg/L	8.146	0.987
Control for 0.1 mg/L	8.336	0.788
Control for 1 mg/L	8.336	0.788
Control for 10 mg/L	8.336	0.788
Control for 50 mg/L	8.146	0.987
0.01 mg/L	7.011	1.397
0.1 mg/L	6.782	2.288
1 mg/L	8.687	1.266
10 mg/L	7.525	2.729
50 mg/L	6.430	0.650
P-PBAT-Olig	Chlorophyl (*a*+*b*), mg/L, mean	Chlorophyl (*a*+*b*), mg/L, SD
Control for 0.01 mg/L	8.146	0.987
Control for 0.1 mg/L	8.336	0.788
Control for 1 mg/L	8.336	0.788
Control for 10 mg/L	8.336	0.788
Control for 50 mg/L	8.146	0.987
0.01 mg/L	8.335	1.749
0.1 mg/L	8.758	1.109
1 mg/L	8.801	1.784
10 mg/L	8.176	2.060
50 mg/L	5.961	0.484

Table S5. *Raw data of fluorescence intensity detected in FITC (525/40 nm) of C. reinhardtii cells stained with the fluorescent probe DHR123 for reactive oxygen species (ROS) indicator and after 72 h exposure to NP/P-PBAT-NPLs & NP/PPBAT-Olig.*

NP-PBAT-NPLs	FITC Signal, mean	FITC Signal, SD
Control for 0.01 mg/L	26935	2595
Control for 0.1 mg/L	27819	2482
Control for 1 mg/L	26093	3366
Control for 10 mg/L	28709	5572
Control for 50 mg/L	28898	1068
0.01 mg/L	34850	4482
0.1 mg/L	32914	5397
1 mg/L	31900	2771
10 mg/L	38858	4565
50 mg/L	44520	7955
P-PBAT-NPLs	FITC Signal, mean	FITC Signal, SD
Control for 0.01 mg/L	21120	684
Control for 0.1 mg/L	22173	2594
Control for 1 mg/L	20966 863	
Control for 10 mg/L	26824 3117	
Control for 50 mg/L	20602 1461	
0.01 mg/L	24769	1964
0.1 mg/L	25531 4387	
1 mg/L	24989	4862
10 mg/L 34040	4871	
50 mg/L	28291	1447
NP-PBAT-Olig	FITC Signal, mean	FITC Signal, SD
Control for 0.01 mg/L	23996	1315
Control for 0.1 mg/L	21518	1700
Control for 1 mg/L	28909	3093
Control for 10 mg/L	28411	2770
Control for 50 mg/L	30,395	1,730
0.01 mg/L	23638	2406
0.1 mg/L	20371	2416
1 mg/L	30819	2163
10 mg/L	33488	4579
50 mg/L	39227	2736
P-PBAT-Olig	FITC Signal, mean	FITC Signal, SD
Control for 0.01 mg/L	21193	2838
Control for 0.1 mg/L	34068	1785
Control for 1 mg/L	48351	8628
Control for 10 mg/L	49510	5130
Control for 50 mg/L	20647	1712
0.01 mg/	21061	3458
0.1 mg/L	34950	855
1 mg/L	48909	6168
10 mg/L	56917	9106
50 mg/L	26332	3578

Table S6. *Raw data of fluorescence intensity detected in FITC (525/40 nm) of C. reinhardtii cells stained with the fluorescent probe $DiBAC_4(3)$ for membrane potential indicator and after 72 h exposure to NP/P-PBAT-NPLs & NP/P-PBAT-Olig.*

NP-PBAT-NPLs	FITC Signal, mean	FITC Signal, SD
Control for 0.01 mg/L	3758	637
Control for 0.1 mg/L	5283	809
Control for 1 mg/L	6313	818
Control for 10 mg/L	7412	105
Control for 50 mg/L	7850	345
0.01 mg/L	3880	595
0.1 mg/L	5111	1152
1 mg/L	6409	951
10 mg/L	9228	895
50 mg/L	12103	2374
P-PBAT-NPLs	FITC Signal, mean	FITC Signal, SD
Control for 0.01 mg/L	2943	384
Control for 0.1 mg/L	5527	545
Control for 1 mg/L	7026	789
Control for 10 mg/L	8244	693
Control for 50 mg/L	5663	819
0.01 mg/L	2893	291
0.1 mg/L	6087	1007
1 mg/L	8082	641
10 mg/L	9499	434
50 mg/L	7400	537
NP-PBAT-Olig	FITC Signal, mean	FITC Signal, SD
Control for 0.01 mg/L	3181	634
Control for 0.1 mg/L	3105	555
Control for 1 mg/L	2990	262
Control for 10 mg/L	2762	184
Control for 50 mg/L	2686	54
0.01 mg/L	3215	417
0.1 mg/L	3244	531
1 mg/L	3300	365
10 mg/L	3136	284
50 mg/L	3418	155
P-PBAT-Olig	FITC Signal, mean	FITC Signal, SD
Control for 0.01 mg/L	2972	345
Control for 0.1 mg/L	2890	307
ontrol for 1 mg/L	2875	200
Control for 10 mg/L	2690	222
Control for 50 mg/L	2630	99
0.01 mg/L	3282	233
0.1 mg/L	3050	500
1 mg/L	3242	543
10 mg/L	3053	454
50 mg/L	3210	481

Table S7. *Raw data of lipid peroxidation, measured by thiobarbituric acid reactive substances method (TBARS) and expressed as µg malondialdehyde (MDA)/mg dry weight (DW), on C. reinhardtii after 72 h exposure to NP/P-PBATNPLs & NP/P-PBAT-Olig.*

NP-PBAT-NPLs	TBARS (µg MDA/mg DW), mean	TBARS (µg MDA/mg DW), SD
Control for 0.01 mg/L	0.030	0.002
Control for 0.1 mg/L	0.030	0.002
Control for 1 mg/L	0.030	0.002
Control for 10 mg/L	0.030	0.002
Control for 50 mg/L	0.030	0.002
0.01 mg/L	0.035	0.004
0.1 mg/L	0.035	0.004
1 mg/L	0.035	0.002
10 mg/L	0.043	0.002
50 mg/L	0.046	0.004
P-PBAT-NPLs	TBARS (µg MDA/mg DW), mean	TBARS (µg MDA/mg DW), SD
Control for 0.01 mg/L	0.030	0.002
Control for 0.1 mg/L	0.030	0.002
Control for 1 mg/L	0.030	0.002
Control for 10 mg/L	0.030	0.002
Control for 50 mg/L	0.030	0.002
0.01 mg/L	0.034	0.005
0.1 mg/L	0.035	0.004
1 mg/L	0.035	0.002
10 mg/L	0.042	0.004
50 mg/L	0.045	0.005
NP-PBAT-Olig	TBARS (µg MDA/mg DW), mean	TBARS (µg MDA/mg DW), SD
Control for 0.01 mg/L	0.030	0.004
Control for 0.1 mg/L	0.030	0.004
Control for 1 mg/L	0.030	0.004
Control for 10 mg/L	0.030	0.004
Control for 50 mg/L	0.030	0.004
0.01 mg/L	0.034	0.004
0.1 mg/L	0.034	0.003
1 mg/L	0.034	0.002
10 mg/L	0.035	0.004
50 mg/L	0.038	0.006
P-PBAT-Olig	TBARS (µg MDA/mg DW), mean	TBARS (µg MDA/mg DW), SD
Control for 0.01 mg/L	0.030	0.004
Control for 0.1 mg/L	0.030	0.004
Control for 1 mg/L	0.030	0.004
Control for 10 mg/L	0.030	0.004
Control for 50 mg/L	0.030	0.004
0.01 mg/L	0.034	0.002
0.1 mg/L	0.034	0.003
1 mg/L	0.034	0.004
10 mg/L	0.035	0.003
50 mg/L	0.038	0.003

Table S8. *Raw data of oxygen evolution expressed as µmol O_2/mg Chlorophyl (a+b) · h of C. reinhardtii after 72 h exposure to NP/P-PBAT-NPLs & NP/PPBAT-Olig.*

NP-PBAT-NPLs	µmol O_2/mg Chlorophyl (*a*+*b*), mean	µmol O_2/mg Chlorophyl (*a*+*b*), SD
Control	225.4	9.5
0.1 mg/L	201.9	15.4
10 mg/L	187.4	2.5
P-PBAT-NPLs	µmol O_2/mg Chlorophyl (*a*+*b*), mean	µmol O_2/mg Chlorophyl (*a*+*b*), SD
Control	225.4	9.5
0.1 mg/L	205.4	7.6
10 mg/L	185.6	19.1
NP-PBAT-Olig	µmol O_2/mg Chlorophyl (*a*+*b*), mean	µmol O_2/mg Chlorophyl (*a*+*b*), SD
Control	232.6	19.4
0.1 mg/L	214.3	3.7
10 mg/L	204.9	17.5
P-PBAT-Olig	µmol O_2/mg Chlorophyl (*a*+*b*), mean	µmol O_2/mg Chlorophyl (*a*+*b*), SD
Control	232.6	19.4
0.1 mg/L	205.3	13.7
10 mg/L	195.9	4.5

Table S9. *Raw data cell size based on flow cytometry back scatter detected with forward scatter FSC of C. reinhardtii cells after 72 h exposure to NP/PPBAT-NPLs & NP/P-PBAT-Olig.*

NP-PBAT-NPLs	FSC, mean	FSC, SD
Control	786,653	19,144
0.1 mg/L	789,255	17,488
10 mg/L	834,648	20,244
P-PBAT-NPLs	FSC, mean	FSC, S
Control	776,479	18,606
0.1 mg/L	783,186	8,697
10 mg/L	822,909	23,747
NP-PBAT-Olig	FSC, mean	FSC, S
Control	1,004,230	139,767
0.1 mg/L	945,057	104,617
10 mg/L	1,000,270	101,500
P-PBAT-Olig	FSC, mean	FSC, S
Control	1,004,230	139,767
0.1 mg/L	945,057	104,617
10 mg/L	1,000,270	101,500

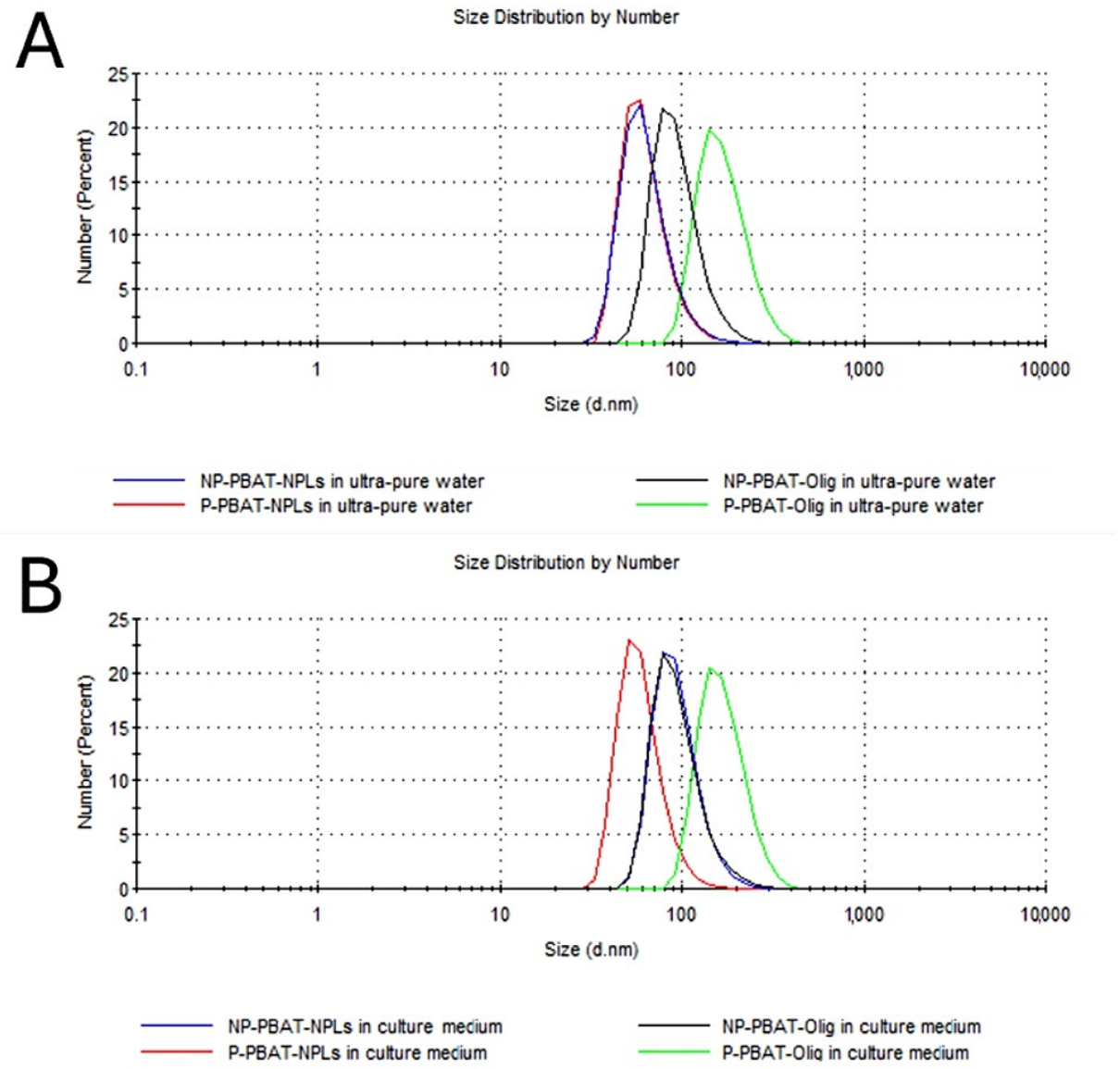

Figure S1: *Hydrodynamic size distribution curves by number (measured by Dynamic Ligth Scattering) of NP- and P-PBAT-NPLs and NP- and PPBAT-Olig in ultrapure water (A). Hydrodynamic size distribution curves by number of NP- and P-PBAT-NPLs and NP- and P-PBAT-Olig in culture medium (B).*

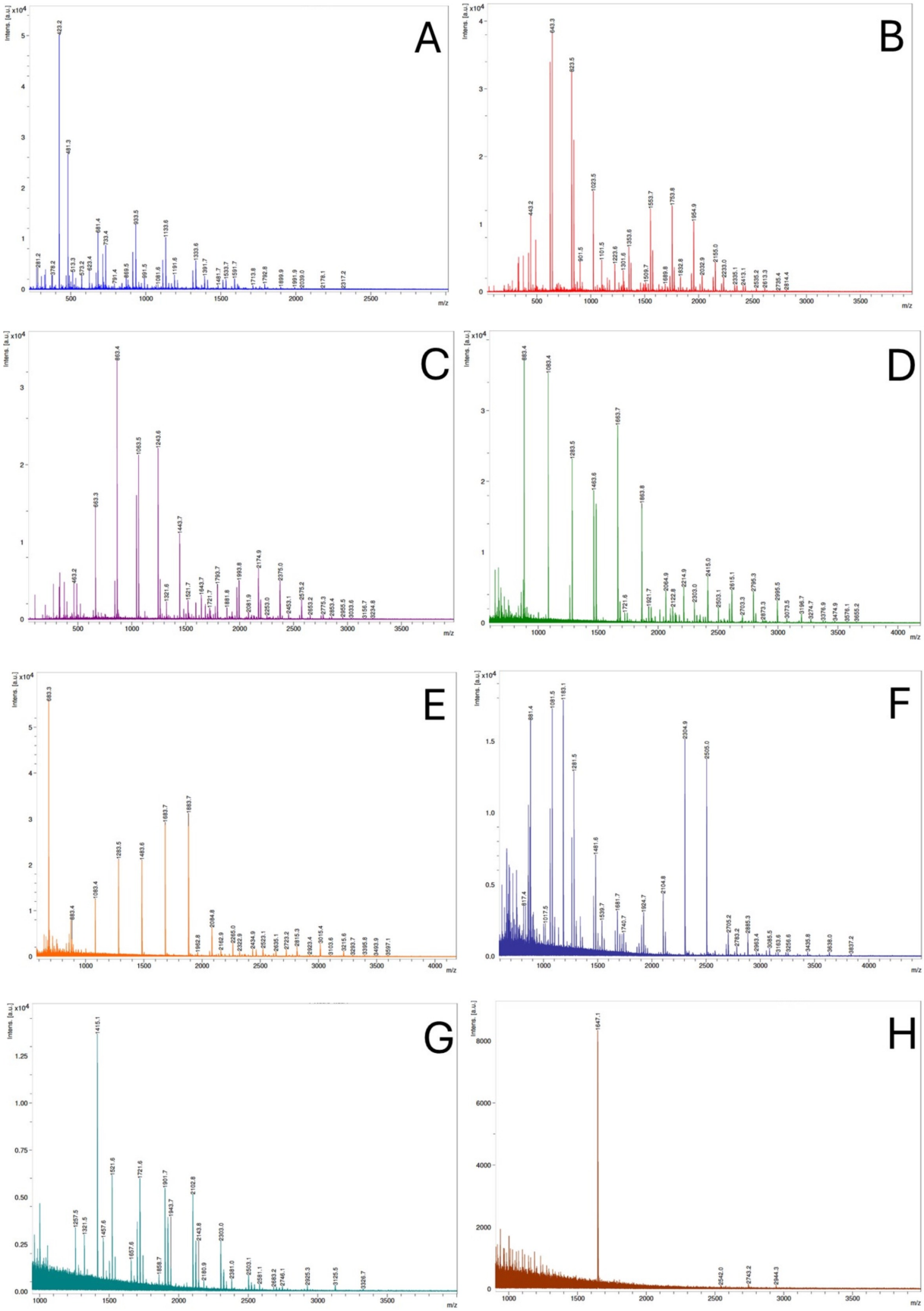

Figure S2: *MALDI-TOF/TOF spectrum of NP-PBAT-Olig chromatography peaks 1(A), 2(B), 3(C), 4(D), 5(E), 6(F), 7(G), and 8 (H).*

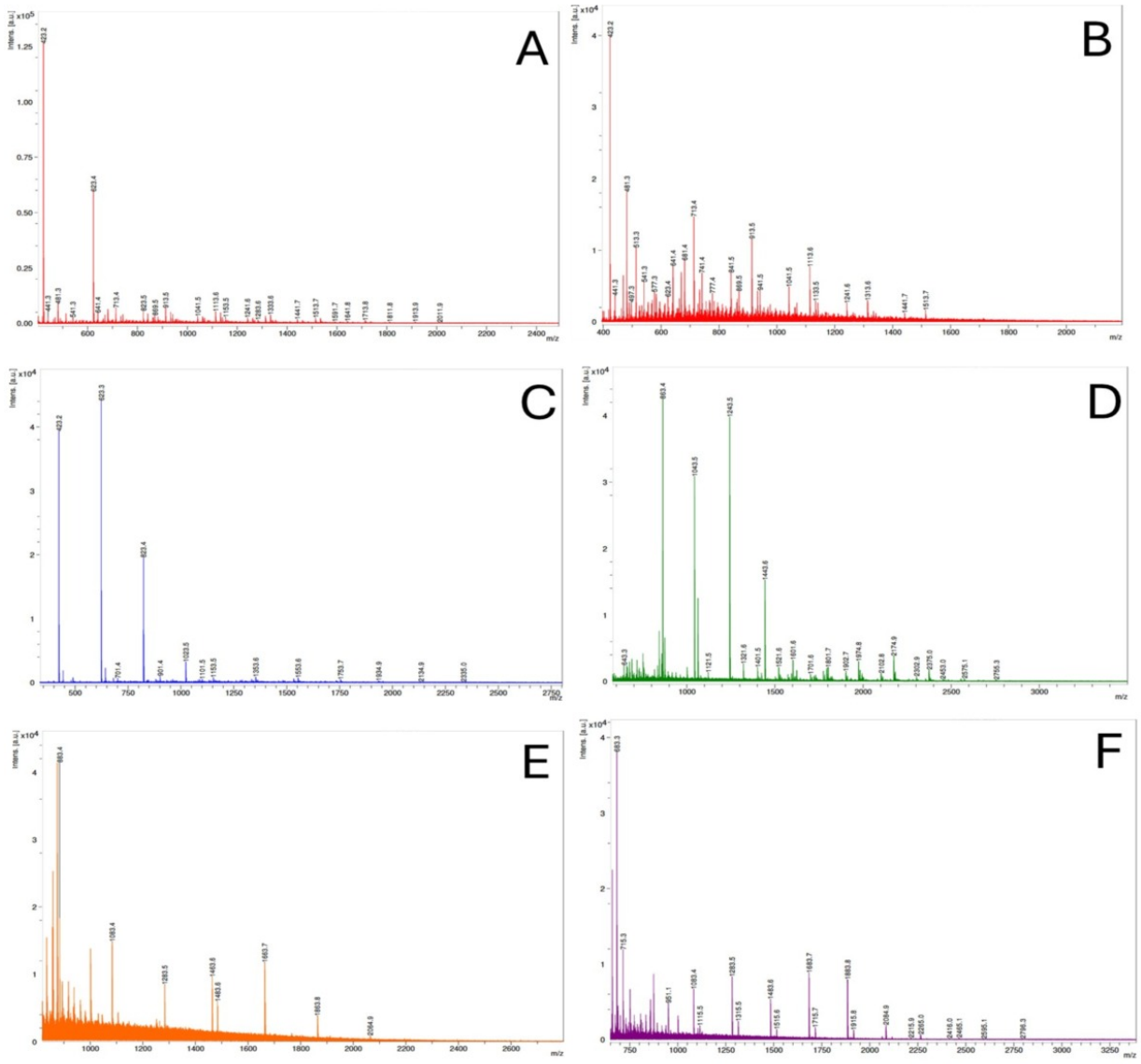

Figure S3: *MALDI-TOF/TOF spectrum of P-PBAT-Olig chromatography peaks 1(A) 2(B), 3(C), 4(D), 5(E), and 6(F).*

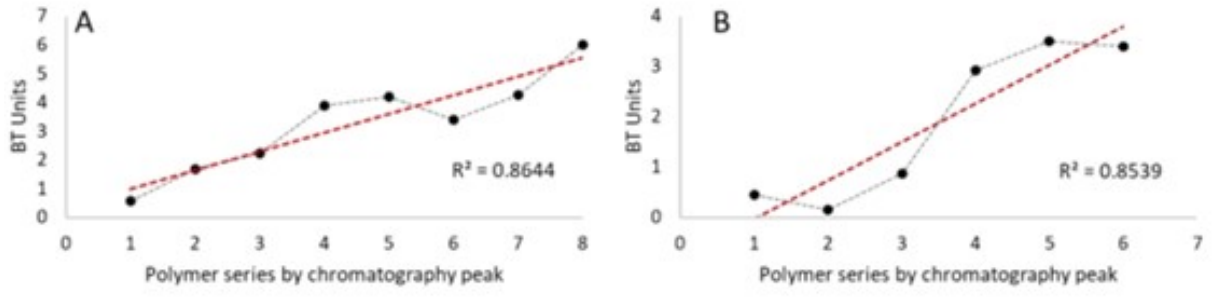

Figure S4: *Mean value of butylene-terephthalate units per polymeric series by chromatography peak (from lower to higher hydrophobicity) of NP- (A) and P- (B) PBAT-Olig.*

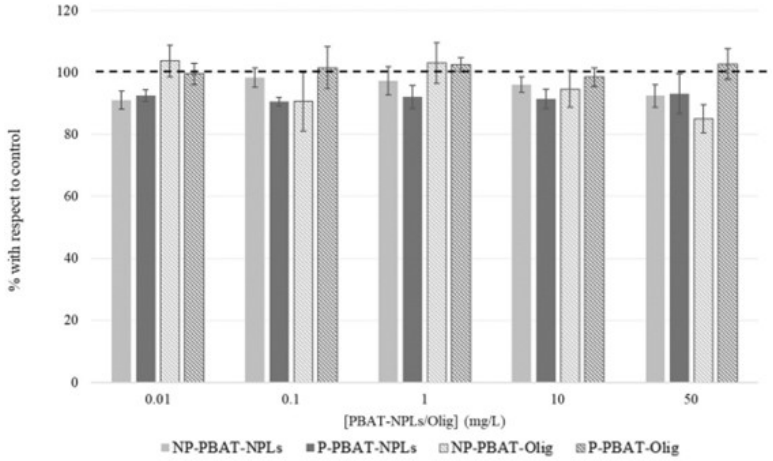

Figure S5: *Growth, expressed as percentage of variation of OD750, on C. reinhardtii after 72 h exposure to NP/P-PBAT-NPLs & NP/P-PBAT-Olig. Asterisks indicate treatments that are significantly different (Dunnet's test, (***) $p < 0.001$.; (**) $p < 0.01$.; (*) $p < 0.05$.) from the control represented as 100 % (dotted line).*

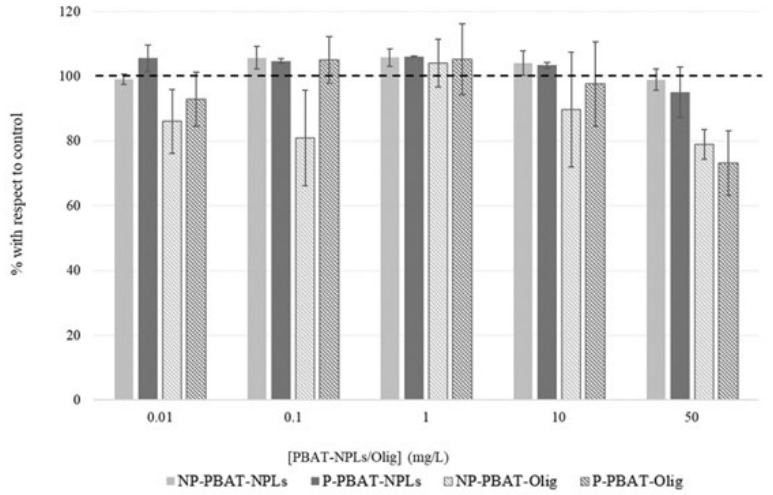

Figure S6: *Representative chlorophyll autofluorescence/bright field overlay images of confocal microscopy of C. reinhardtii after 72 h exposure to NP- and P-PBAT-NPLs. Image shows confocal microscopy images of the non-exposed cells (A and D); cells exposed to 0.1 and 10 mg/L of NP-PBAT-NPLs (B and C, respectively); cells exposed to 0.1 and 10 mg/L of P-PBAT-NPLs (E and F, respectively).*

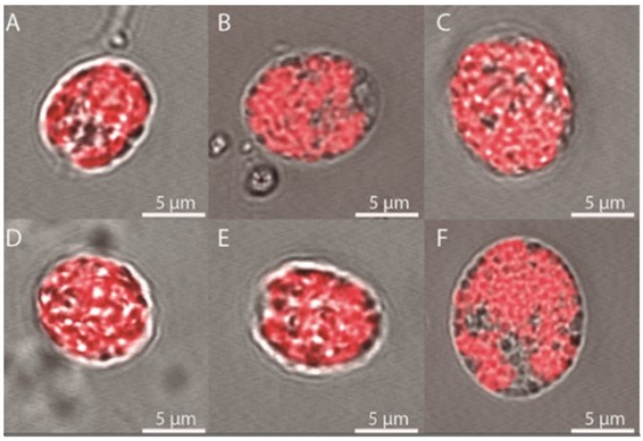

Figure S7: *Representative chlorophyll autofluorescence/bright field overlay images of confocal microscopy of C. reinhardtii after 72 h exposure to NP- and P-PBAT-NPLs. Image shows confocal microscopy images of the non-exposed cells (A and D); cells exposed to 0.1 and 10 mg/L of NP-PBAT-NPLs (B and C, respectively); cells exposed to 0.1 and 10 mg/L of P-PBAT-NPLs (E and F, respectively).*